

---

# Goal-Oriented Sequential Bayesian Experimental Design for Causal Learning

---

Zheyu Zhang<sup>1,\*</sup> Jiayuan Dong<sup>2,\*</sup> Jie Liu<sup>1,3</sup> Xun Huan<sup>2</sup>

<sup>1</sup>Department of Computer Science and Engineering

<sup>2</sup>Department of Mechanical Engineering

<sup>3</sup>Gilbert S. Omenn Department of Computational Medicine and Bioinformatics  
University of Michigan  
Ann Arbor, MI, 48109

{zheyuz, jiayuand, drjeliu, xhuan}@umich.edu

## Abstract

We present GO-CBED, a goal-oriented Bayesian framework for sequential causal experimental design. Unlike conventional approaches that select interventions aimed at inferring the full causal model, GO-CBED directly maximizes the expected information gain (EIG) on user-specified causal quantities of interest, enabling more targeted and efficient experimentation. The framework is both non-myopic, optimizing over entire intervention sequences, and goal-oriented, targeting only model aspects relevant to the causal query. To address the intractability of exact EIG computation, we introduce a variational lower bound estimator, optimized jointly through a transformer-based policy network and normalizing flow-based variational posteriors. The resulting policy enables real-time decision-making via an amortized network. We demonstrate that GO-CBED consistently outperforms existing baselines across various causal reasoning and discovery tasks—including synthetic structural causal models and semi-synthetic gene regulatory networks—particularly in settings with limited experimental budgets and complex causal mechanisms. Our results highlight the benefits of aligning experimental design objectives with specific research goals and of forward-looking sequential planning.

## 1 Introduction

A structural causal model (SCM) provides a mathematical framework for representing causal relationships via a directed acyclic graph (DAG). SCMs are foundational across domains such as genomics and precision medicine [58], economics [64], and the social sciences [55, 33], where understanding the cause-effect relationships is central to scientific inquiry. Key tasks in causal modeling include: *causal discovery*, which learns the DAG structure; *causal mechanism identification*, which estimates functional dependencies; and *causal reasoning*, which answers interventional and counterfactual queries. All such tasks depend on data. While (passive) observational data can reveal correlational structures, they often fail to identify the true causal model [65]. In contrast, (active) *interventional* data are essential for uncovering causal relationships and estimating causal effects—but such experiments are inherently expensive and limited, making careful experimental design essential.

A Bayesian approach to optimal experimental design (BOED) [37, 13, 51, 32] addresses this challenge by selecting interventions that maximize the expected information gain (EIG). BOED provides a principled framework for handling uncertainty in both causal structure and mechanisms. However, most existing causal BOED methods focus on *learning the full model*—for causal discovery or mechanism identification—regardless of the scientific goal.

---

\*Equal contribution.

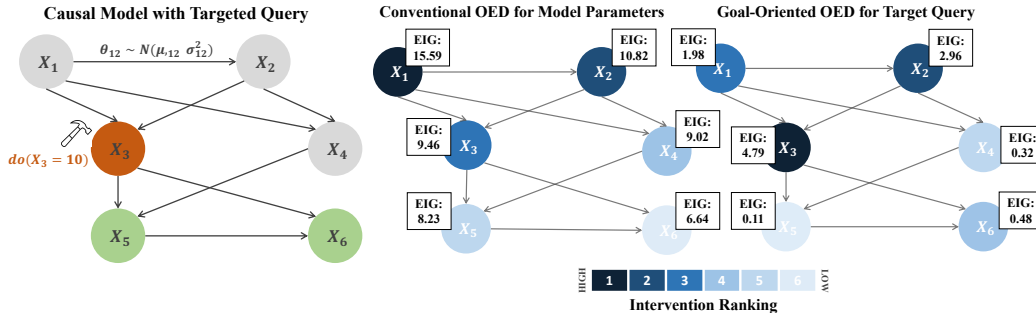


Figure 1: Illustration of goal-oriented versus conventional BOED for causal learning. *Left*: A linear Gaussian SCM with six nodes; the experimental goal is to estimate the causal effect of the intervention  $do(X_3 = 10)$  on node  $X_5$  and  $X_6$ . *Middle*: Conventional BOED selects interventions that maximize EIG over all model parameters, resulting in  $X_1$  and  $X_2$  being selected as the best. *Right*: Our GO-CBED approach selects interventions by directly maximizing EIG for the specific causal query, leading to a different intervention that prioritizes nodes most relevant to the query, i.e.,  $X_3$  and  $X_2$ .

In many real-world applications, the objective is more focused on *causal reasoning*: researchers aim to estimate the effect of a specific intervention, rather than recover the entire causal system. For instance, in drug discovery, it is often more important to understand how particular molecular targets influence disease pathways than to map the full biological network. Shown in Figure 1, optimizing for full model parameters (middle) leads to experiments that are misaligned with such targeted goals (left), resulting in inefficient use of resources (compared to right). This motivates a **goal-oriented** approach to BOED—one that tailors interventions to the specific causal queries that matter the most.

Recent work by Toth et al. [63] begins to address goal-oriented causal design, but adopts a myopic strategy—selecting only the next experiment without planning ahead. More broadly, most causal BOED approaches are greedy, optimizing interventions one step at a time without accounting for how early decisions influence future learning. Overcoming this limitation requires a *non-myopic* framework, which we formulate as a Markov decision process and solve using tools from reinforcement learning (RL) [51, §4], [32, §5].

To address these challenges, we propose **Goal-Oriented Causal Bayesian Experimental Design (GO-CBED)**, a novel framework for sequential, non-myopic causal experimental design that:

- **Directly targets user-defined causal queries**, using a variational lower-bound estimator [50, 7] to efficiently approximate the EIG on these specific quantities of interest (QoIs);
- **Plans non-myopically** across full experimental sequences via a learned RL policy;
- **Enables real-time intervention selection** through an amortized transformer-based policy, trained offline for fast deployment.

Our key contributions include: a **goal-oriented framework** that substantially improves experimental efficiency for specific causal queries; a **sequential, non-myopic strategy** that captures synergies between interventions; and empirical results showing that **GO-CBED outperforms existing methods**.

## 2 Related Work

GO-CBED builds upon and synthesizes advances from three key areas: causal BOED, goal-oriented BOED, and non-myopic sequential BOED.

Early work in causal BOED demonstrated the utility of active interventions for efficiently uncovering causal graph structures, moving beyond passive observational learning [43, 62, 14, 44, 66, 57]. Subsequent research expanded to learning full SCMs, including the selection of both intervention targets and values [61, 60]. More recent work has highlighted the importance of tailoring experiments to specific causal QoIs [63]. However, many of these approaches remain myopic—focusing on single-step gains—or are oriented toward global fidelity rather than user-specific causal objectives.

In parallel, the broader BOED literature has seen growing interest in goal-oriented design, where experiments are optimized for their utility to downstream tasks [5, 68, 69, 12]. These methods have shown substantial benefits in predictive settings, particularly with complex nonlinear models. However, they generally do not address the unique challenges of causal inference, including the interventional nature of learning and the structural constraints of SCMs.

Recognizing the limitations of greedy approaches, non-myopic sequential BOED seeks to optimize entire experimental trajectories rather than one step at a time. Approaches based on amortized policy learning and RL [20, 10, 53, 52] have shown promise in this area. Yet in the causal setting, non-myopic strategies often focus solely on structure learning [3, 24] and do not integrate flexible, user-defined causal goals into the long-term optimization framework.

GO-CBED bridges these domains by introducing a non-myopic, goal-oriented approach to sequential experimental design in causal settings. It enables strategic planning of intervention sequences explicitly optimized to answer user-specified causal queries—such as estimating particular effects or critical mechanisms—within complex SCMs. Unlike prior methods that are goal-oriented but myopic [63] or non-myopic but focused on structure learning [3, 24], GO-CBED unifies both objectives, maximizing long-term utility for causal reasoning. A more comprehensive discussion of related work is provided in Appendix B.

### 3 Preliminaries

**Structural Causal Models** SCMs [46] provide a rigorous mathematical framework for representing and reasoning about cause-effect relationships. An SCM defines a collection of random variables  $\mathbf{X} = \{X_1, \dots, X_d\}$ , structured by a DAG  $G := \{\mathbf{V}, E\}$ . The SCM is denoted as  $\mathcal{M} := \{G, \boldsymbol{\theta}\}$ , where  $G$  encodes the causal structure and  $\boldsymbol{\theta}$  parameterizes the causal mechanisms. Each variable  $X_i$  is determined by its parents in the graph and an exogenous noise term via a structural equation:

$$X_i = f_i(\mathbf{X}_{\text{pa}(i)}, \boldsymbol{\theta}_i; \epsilon_i), \quad \forall i \in \mathbf{V}. \quad (1)$$

Here,  $\mathbf{X}_{\text{pa}(i)}$  denotes the parent variables of  $X_i$  in  $G$ ,  $f_i$  is a causal mechanism parameterized by  $\boldsymbol{\theta}_i$ , and  $\epsilon_i \sim P_{\epsilon_i}$  is an independent noise variable. The SCM thus defines a joint distribution over  $\mathbf{X}$ , enabling causal reasoning and interventional analysis.

**Interventions (Experimental Designs)** SCMs support formal reasoning about interventions—i.e., external manipulations to the system. A *perfect* (or *hard*) intervention on a subset of variables  $\mathbf{X}_I$ , denoted by  $\text{do}(\mathbf{X}_I = s_I)$  [46], replaces the corresponding structural equations with fixed values  $s_I$ , modifying the data-generation process. This introduces an *interventional SCM*, which leads to a new distribution over the variables. Assuming causal sufficiency and independent noise [56], the interventional distribution follows the Markov factorization:

$$p(\mathbf{X} | \mathcal{M}, \boldsymbol{\xi}) = \prod_{j \in \mathbf{V} \setminus I} p(X_j | \mathbf{X}_{\text{pa}(j)}, \boldsymbol{\theta}_j, \text{do}(\mathbf{X}_I = s_I)), \quad (2)$$

where the design variable  $\boldsymbol{\xi} := \{I, s_I\}$  encodes both the intervention target  $I$  and the intervention value  $s_I$ . Interventions form the foundation for both causal discovery (i.e., identifying  $G$ ) and causal reasoning (i.e., estimating interventional effects).

**Goal-Oriented Sequential Bayesian Framework** Conventional causal BOED methods typically follow a two-step procedure: first, learn the full model, and then use it to answer causal queries. Such an approach can be inefficient when only a small subset of causal QoIs matter, as it may spend significant resources learning aspects of the model irrelevant to the target queries.

To address this inefficiency, we adopt a goal-oriented perspective: rather than learning the entire model, we design experiments to directly improve our ability to answer specific causal queries. We formalize this using a query function  $H$  that maps the causal model  $\mathcal{M}$  to the desired quantity  $z = H(\mathcal{M}; \epsilon_z)$ , where  $\epsilon_z$  captures any inherent stochasticity in the query. For example, setting  $z = G$  corresponds to causal discovery, while  $z = X_i^{\text{do}(X_j = \psi_j)}$  corresponds to estimating the causal effect of setting  $X_j = \psi_j$  on  $X_i$  from a distribution of possible intervention values  $\psi_j \sim p(\psi_j)$ .

At experiment stage  $t$  of a sequence of  $T$  experiments, let the history be  $\mathbf{h}_t := \{\boldsymbol{\xi}_{1:t}, \mathbf{x}_{1:t}\}$ , where  $\boldsymbol{\xi}_\tau$  and  $\mathbf{x}_\tau$  denote the design and outcome of the  $\tau$ -th interventional experiment. The belief over the

causal model  $\mathcal{M} = \{G, \theta\}$  is updated via Bayes' rule:<sup>2</sup>

$$p(G|\mathbf{h}_t) = \frac{p(G|\mathbf{h}_{t-1})p(\mathbf{x}_t|G, \mathbf{h}_{t-1}, \boldsymbol{\xi}_t)}{p(\mathbf{x}_t|\mathbf{h}_{t-1}, \boldsymbol{\xi}_t)}, \quad p(\theta|G, \mathbf{h}_t) = \frac{p(\theta|G, \mathbf{h}_{t-1})p(\mathbf{x}_t|G, \theta, \mathbf{h}_{t-1}, \boldsymbol{\xi}_t)}{p(\mathbf{x}_t|G, \mathbf{h}_{t-1}, \boldsymbol{\xi}_t)},$$

where the marginal likelihood  $p(\mathbf{x}_t|G, \mathbf{h}_{t-1}, \boldsymbol{\xi}_t)$  is computed by integrating over  $\theta$ . However, our primary interest lies not in inferring the full model  $\mathcal{M}$ , but in updating beliefs about the target query  $\mathbf{z}$ . This is captured by the posterior-predictive distribution:

$$p(\mathbf{z}|\mathbf{h}_t) = \sum_G \int p(\mathbf{z}|G, \theta, \mathbf{h}_t) p(G|\mathbf{h}_t) p(\theta|G, \mathbf{h}_t) d\theta. \quad (3)$$

## 4 Goal-Oriented Sequential Causal Bayesian Experimental Design

**Problem Statement** GO-CBED seeks an optimal policy  $\pi : \mathbf{h}_{t-1} \rightarrow \boldsymbol{\xi}_t$  that maximizes the EIG on the target causal QoI  $\mathbf{z}$  over a sequence of  $T$  experiments:

$$\pi^* \in \arg \max_{\pi} \left\{ \mathcal{I}_T(\pi) := \mathbb{E}_{p(\mathcal{M})p(\mathbf{h}_T|\mathcal{M}, \pi)p(\mathbf{z}|\mathcal{M})} \left[ \log \frac{p(\mathbf{z}|\mathbf{h}_T)}{p(\mathbf{z})} \right] \right\}, \quad (4)$$

subject to the constraint that designs following the policy:  $\boldsymbol{\xi}_t = \pi(\mathbf{h}_{t-1})$  for all  $t$ . This formulation is *goal-oriented*, as it directly targets EIG on specific causal QoIs rather than the full model, and *non-myopic*, as it optimizes the entire sequence of interventions rather than selecting each greedily. An equivalent formulation based on incremental (stage-wise) EIG after each experiment is also possible; see Appendix A.1 for details.

The EIG on  $\mathbf{z}$  defined in (4),  $\mathcal{I}_T$ , is also the mutual information between  $\mathbf{z}$  and  $\mathbf{h}_T$ . When  $\mathbf{z}$  is a bijective function of  $\mathcal{M}$ , maximizing EIG on  $\mathbf{z}$  is equivalent to maximizing it on  $\mathcal{M}$  [8]. However, when  $\mathbf{z}$  is not invertible with respect to  $\mathcal{M}$ , directly maximizing EIG on  $\mathbf{z}$  becomes more efficient. It avoids expending effort on irrelevant parts of  $\mathcal{M}$ , reducing both computational and experimental costs—especially beneficial when dealing with large causal graphs or tight intervention budgets.

### 4.1 Variational Lower Bound

Evaluating and optimizing the EIG in (4) requires estimating the posterior density  $p(\mathbf{z}|\mathbf{h}_T)$ , which is generally intractable for complex causal models. To address this, we adopt a *variational approach* that approximates the posterior using  $q_{\boldsymbol{\lambda}}(\mathbf{z}|\pi, f_{\phi}(\mathbf{h}_T))$ , where  $\boldsymbol{\lambda}$  is the variational parameter and  $f_{\phi}$  is a learned embedding of the historical interventional data:

$$\mathcal{I}_{T;L}(\pi; \boldsymbol{\lambda}, \phi) := \mathbb{E}_{p(\mathcal{M})p(\mathbf{h}_T|\mathcal{M}, \pi)p(\mathbf{z}|\mathcal{M})} \left[ \log \frac{q_{\boldsymbol{\lambda}}(\mathbf{z}|f_{\phi}(\mathbf{h}_T))}{p(\mathbf{z})} \right], \quad (5)$$

subject to  $\boldsymbol{\xi}_t = \pi(\mathbf{h}_{t-1})$  for all  $t$ .

**Theorem 4.1** (Variational Lower Bound). *For any policy  $\pi$ , variational parameter  $\boldsymbol{\lambda}$ , and embedding parameter  $\phi$ , the EIG satisfies  $\mathcal{I}_T(\pi) \geq \mathcal{I}_{T;L}(\pi; \boldsymbol{\lambda}, \phi)$ . The bound is tight if and only if  $p(\mathbf{z}|\mathbf{h}_T) = q_{\boldsymbol{\lambda}}(\mathbf{z}|f_{\phi}(\mathbf{h}_T))$  for all  $\mathbf{z}$  and  $\mathbf{h}_T$ .*

A proof is provided in Appendix A.2. Since  $p(\mathbf{z})$  is independent of  $\pi$ ,  $\boldsymbol{\lambda}$ , and  $\phi$ , it can be omitted from the optimization statement without affecting the argmax. Thus, maximizing the EIG lower bound reduces to maximizing the *prior-omitted* EIG bound:

$$\pi^*, \boldsymbol{\lambda}^*, \phi^* \in \arg \max_{\pi, \boldsymbol{\lambda}, \phi} \left\{ \mathcal{R}_{T;L}(\pi; \boldsymbol{\lambda}, \phi) := \mathbb{E}_{p(\mathcal{M})p(\mathbf{h}_T|\mathcal{M}, \pi)p(\mathbf{z}|\mathcal{M})} [\log q_{\boldsymbol{\lambda}}(\mathbf{z}|f_{\phi}(\mathbf{h}_T))] \right\}, \quad (6)$$

where  $\mathcal{R}_{T;L}(\pi; \boldsymbol{\lambda}, \phi) \leq \mathcal{R}_T(\pi) := \mathbb{E}_{p(\mathcal{M})p(\mathbf{h}_T|\mathcal{M}, \pi)p(\mathbf{z}|\mathcal{M})} [\log p(\mathbf{z}|\mathbf{h}_T)]$  is a lower bound to the prior-omitted EIG  $\mathcal{R}_T(\pi)$ . See Appendix A.3 for additional information on  $\mathcal{R}_{T;L}(\pi; \boldsymbol{\lambda}, \phi)$ .

<sup>2</sup>When observational data  $\mathcal{D}$  is available prior to designing interventions, all distributions are implicitly conditioned on  $\mathcal{D}$ . See Appendix C.4 for further details.

## 4.2 Variational Posteriors and Policy Network

Having established the theoretical foundation of GO-CBED, we now describe its implementation. Our approach comprises two key components: (1) variational posteriors for establishing the EIG lower bound, and (2) a policy network that guides the intervention selection process.

**Variational Posteriors** While GO-CBED supports arbitrary causal queries, we focus on two fundamental tasks that form the basis of our experimental evaluation: causal reasoning (i.e., estimating interventional effects) and causal discovery (i.e., learning graph structure).

For causal reasoning tasks, where the query takes the form  $\mathbf{z} = X_i^{\text{do}(X_j=\psi_j)}$ , the posterior distribution  $p(\mathbf{z}|\mathbf{h}_T)$  is often complex and multimodal due to the structural uncertainty—different causal graphs can imply different causal effects for the same intervention. To capture this complexity, we parameterize the variational posterior  $q_\lambda(\mathbf{z}|f_\phi(\mathbf{h}_T))$  using normalizing flows (NFs), which transform a Gaussian base distribution into a flexible target distribution via a series of invertible mappings, while enabling efficient density estimation. Specifically, we use the Real NVP architecture [18] and follow the implementation strategy of Dong et al. [19]. Details are provided in Appendix A.4.

For causal discovery tasks, where the query is the graph itself,  $\mathbf{z} = G$ , we model the posterior over graph structures using an independent Bernoulli distribution for each potential edge [41]:

$$q_\lambda(G|f_\phi(\mathbf{h}_T)) = \prod_{i,j} q_\lambda(G_{i,j}|f_\phi(\mathbf{h}_T)), \quad (7)$$

where each  $q_\lambda(G_{i,j}|\cdot) \sim \text{Bernoulli}(\lambda_{i,j})$ . This parameterization allows efficient modeling of the posterior over DAG structures, while maintaining scalability and differentiability.

**Policy Network** We represent the policy  $\pi$  using a neural network with parameters  $\gamma$ . The policy network selects the next intervention by mapping the history  $\mathbf{h}_{t-1}$  to a design  $\xi_t$  at stage  $t$ . The architecture is designed to satisfy two symmetry properties that have been shown to improve performance [3]: permutation invariance across history samples and permutation equivariance across variables.

The network is composed of  $L$  transformer layers that alternate between attention over variable and observation dimensions. This alternating structure enables rich and efficient information flow across the entire history of interventions and outcomes. The final embedding is passed through two output heads: one that produces the intervention targets  $I_t$ , using the Gumbel-softmax trick to enable differentiability for discrete variables, and the other predicts the corresponding intervention values  $s_{I_t}$ . The architecture is illustrated in Appendix C.1.

**Training Procedure** Algorithm 1 outlines our training procedure, which jointly optimizes the policy parameters and variational parameters by maximizing the variational lower bound. In each training iteration, we sample causal models  $\mathcal{M} = (G, \theta)$  from the prior, derive the target QoIs  $\mathbf{z}$ , simulate intervention trajectories, and update all network parameters via gradient ascent. At deployment time, only forward passes through the policy network are required, eliminating the need for online Bayesian inference. This enables real-time decision-making with constant computational complexity, independent of experiment sequence length.

---

### Algorithm 1 The GO-CBED algorithm.

---

- 1: **Input:**  $H, p(\psi)$ ; prior  $p(G), p(\theta|G)$ ; likelihood  $p(\mathbf{x}_t|G, \theta, \xi_t)$ ; number of experiments  $T$ ;
  - 2: Initialize policy network parameters  $\gamma$ , variational parameters  $\lambda$ , embedding parameters  $\phi$ ;
  - 3: **for**  $l = 1, \dots, n_{\text{step}}$  **do**
  - 4:   Simulate  $n_{\text{env}}$  samples of  $G, \theta, \psi$  and  $\mathbf{z}$ ;
  - 5:   **for**  $t = 0, \dots, T$ , **do**
  - 6:     Compute  $\xi_t = \pi(\mathbf{h}_{t-1})$ , then sample  $\mathbf{x}_t \sim p(\mathbf{x}_t|G, \theta, \xi_t)$ ;
  - 7:   **end for**
  - 8:   Update  $\gamma, \lambda$ , and  $\phi$  following gradient ascent, where gradient obtained from auto-grad on  $\mathcal{R}_{T;L}$ ;
  - 9: **end for**
  - 10: **Output:** Optimal  $\pi^*$  parameterized by  $\gamma^*$ , and  $\lambda^*$ , and  $\phi^*$ ;
-

## 5 Numerical Results

Our numerical experiments demonstrate how GO-CBED advances causal experimental design through goal-oriented optimization. We begin in Section 5.1 to recap the motivating example from Figure 1 that illustrates the fundamental advantage of targeting specific causal queries over full model learning. We then focus on two key causal tasks: Section 5.2 examines causal reasoning, where we evaluate performance in estimating targeted causal effects across both synthetic causal models and semi-synthetic gene regulatory networks derived from the Dialogue for Reverse Engineering Assessments and Methods (DREAM) benchmarks [27]; Section 5.3 then turns to causal discovery, comparing GO-CBED against existing causal BOED baselines on similar synthetic and semi-synthetic settings.

### 5.1 Motivating Example with Fixed Graph Structure

We first evaluate the benefits of goal-oriented policies on the motivating example with a fixed graph structure in Figure 1. This setup assumes a linear-Gaussian relationship between variables, allowing for analytical posterior computation and accurate EIG estimation. We compare four policies: **GO-CBED- $z$** , which is optimized for the specific causal query; **GO-CBED- $\theta$** , which targets model parameters; **NMC**, a baseline that uses the nested Monte Carlo (NMC) estimator for the prior-omitted EIG on QoIs [63]; and **Random**, which selects both intervention targets and values uniformly at random. We evaluate their performance on the prior-omitted EIG (or lower bound) for  $z$ . Full experiment details can be found in Appendix C.2.

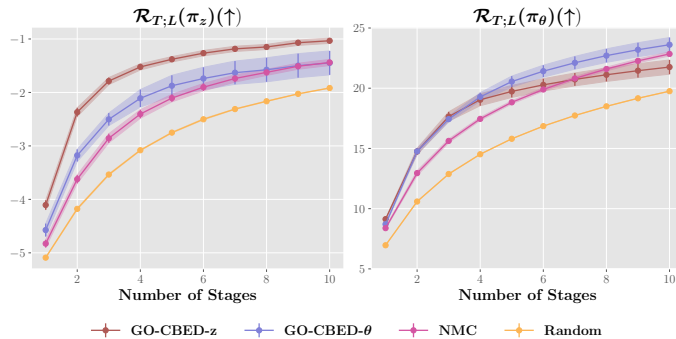


Figure 2: Performance comparison of policies trained for  $T = 10$ , evaluated across different stage lengths. *Left*: Performance on causal query  $z = \{X_5, X_6 \mid \text{do}(X_3 = 10)\}$ . *Right*: Performance on model parameters  $z = \{\theta \setminus \theta_{\text{pa}(3)}\}$ . While GO-CBED- $\theta$  achieves higher EIG on the task centering parameters (right), it performs significantly worse than GO-CBED- $z$  on the causal reasoning task (left). Shaded regions represent  $\pm 1$  standard error across 4 random seeds.

Figure 2 reveals a key insight: although GO-CBED- $\theta$  achieves higher EIG on model parameters, its performance on the actual causal query is substantially worse than that of GO-CBED- $z$ . This supports our central argument—when the goal is to answer specific causal queries, policies that directly target those queries are significantly more efficient than those optimized for general model learning. Moreover, GO-CBED’s variational formulation consistently outperforms the sampling-based NMC. This advantage is especially pronounced when the inner-loop sample size in NMC is small, where the estimator suffers from high bias (see Appendix D.1).

### 5.2 Causal Reasoning Tasks

We evaluate GO-CBED’s ability to design interventions that maximize EIG with respect to specific causal queries, now no longer fixing the graph structure. We compare three policies: **GO-CBED- $z$**  optimized directly for causal queries, **GO-CBED- $G$**  trained for causal discovery, and **Random** selection. Additional experiment details are provided in Appendix C.3.

**Synthetic SCMs** Figure 3 compares performance using Erdős-Rényi (ER) and Scale-Free (SF) graph priors with linear and nonlinear mechanisms, detailed in Appendix C.3. In linear settings, GO-CBED- $z$  and GO-CBED- $G$  perform similarly, indicating that causal structure alone is often sufficient to accurately estimate simple causal effects. However, in nonlinear settings, GO-CBED- $z$  significantly outperforms GO-CBED- $G$ , despite the latter’s strong performance on causal discovery tasks (see Appendix C.3). These results indicate a key insight: as the complexity of causal mechanisms increases, directly targeting causal queries becomes increasingly advantageous. Moreover, in nonlinear mechanisms parameterized by neural networks, the dimensionality of the weights  $\theta$

is large and graph-dependent, making it challenging to generate sufficient samples to effectively tighten the EIG lower bound for full graphs and parameters. These are precisely the advantages that goal-oriented design aims to provide.

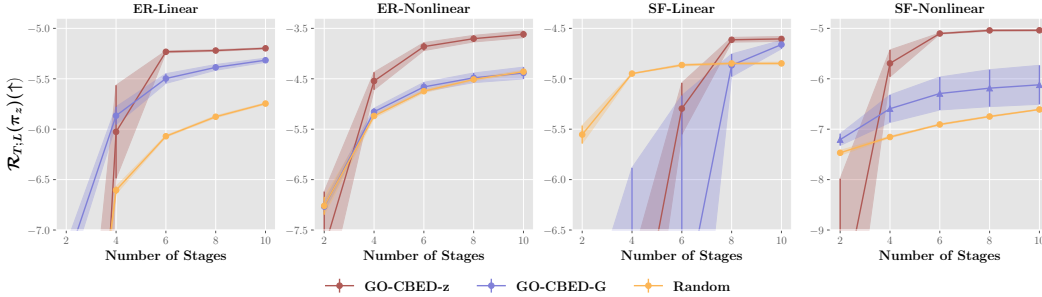


Figure 3: Performance comparison of policies trained for  $T = 10$  on causal queries, using ER and SF graph priors with linear and nonlinear mechanisms (3 interventions per stage,  $d = 10$ ). While GO-CBED- $G$ —which targets structure learning—is a natural baseline, it underperforms on causal queries, particularly in nonlinear settings. In contrast, GO-CBED- $z$ , which directly targets causal QoI, consistently achieves higher EIG, especially under nonlinear mechanisms. Shaded regions represent  $\pm 1$  standard error over 4 random seeds.

### Semi-Synthetic Gene Regulatory Networks

To assess real-world applicability, we evaluate GO-CBED on semi-synthetic gene regulatory networks derived from the DREAM [27] benchmarks, detailed in Appendix C.3. Figure 4 presents results on *E. coli* networks with nonlinear causal mechanisms ( $d = 10, T = 10$ ). GO-CBED- $z$ , which directly targets causal query, significantly outperforms both GO-CBED- $G$  and Random baselines, especially after the initial stages of intervention. In addition, GO-CBED- $G$  performs worse than Random despite achieving better causal discovery performance (see Appendix C.3), indicating that recovering the causal graph does not necessarily provide good uncertainty reduction for specific causal queries. This performance gap on biologically-inspired networks has important practical implications. In real biological research, experimental resources are often limited, and researchers typically seek to answer specific causal questions rather than infer the entire network structure. GO-CBED’s ability to efficiently target such queries highlights its promise for applications such as gene regulatory network analysis and drug target identification, where maximizing information about specific causal effects is critical. We further validate GO-CBED’s effectiveness through additional experiments on Yeast networks and with diverse goal specifications in Appendix D.2. Additional evaluations of GO-CBED’s robustness to distributional shifts in observation noise are presented in Appendix D.5.

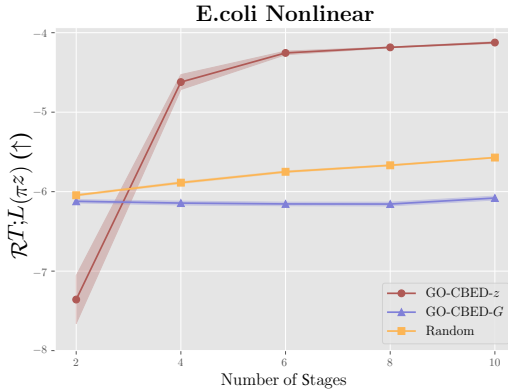


Figure 4: Performance comparison of policies trained for  $T = 10$  on *E. coli* gene regulatory networks with nonlinear causal mechanisms ( $d = 10$ ). GO-CBED- $z$  performs comparably to baselines in early stages but exhibits rapid improvement after stage 3, ultimately achieving substantially higher EIG than both GO-CBED- $G$  and Random. These results highlight the value of goal-oriented experimental design in realistic biological settings with complex nonlinear causal mechanisms. Shaded regions represent  $\pm 1$  standard error across 4 random seeds.

### 5.3 Causal Discovery Tasks

While GO-CBED is primarily designed for general goal-oriented experimental design, we also apply it to specific causal discovery tasks, where the target QoI is the causal graph  $z = G$ . This enables comparison with existing causal BOED methods specifically designed for structure learning. We

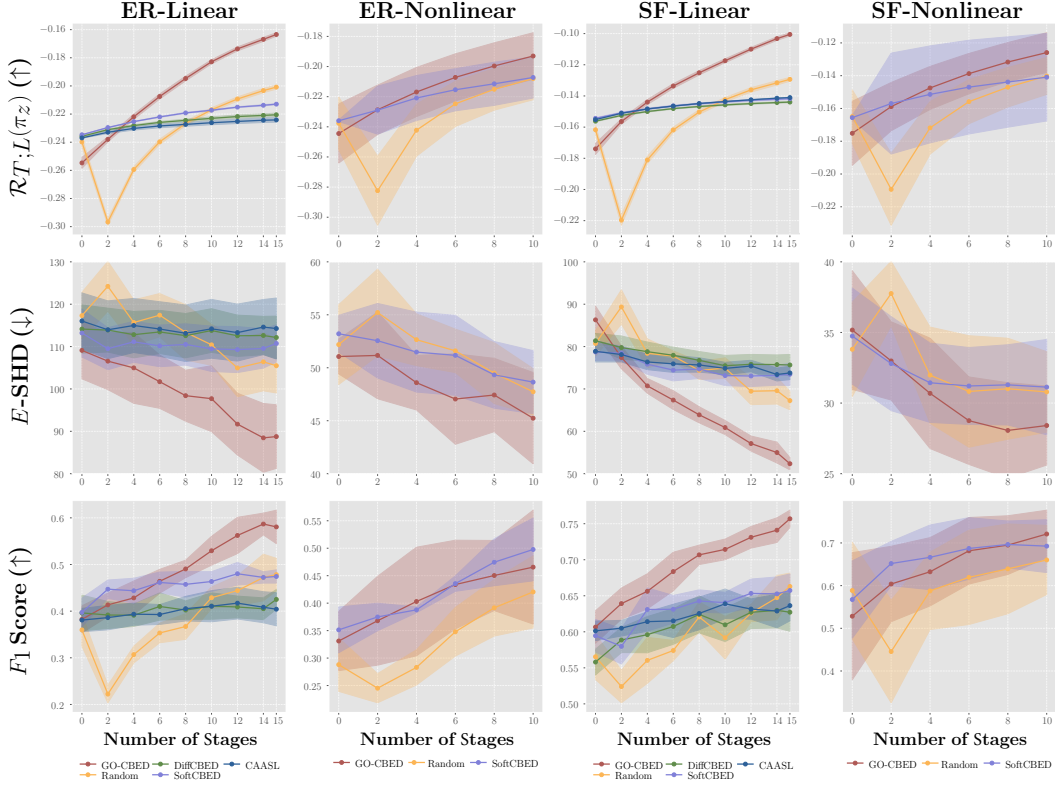


Figure 5: Performance comparison on synthetic SCMs, using ER and SF graph priors with linear and nonlinear mechanisms. Metrics include prior-omitted EIG lower bound  $\mathcal{R}_{T;L}$ , expected structural Hamming distance  $\mathbb{E}$ -SHD, and  $F_1$ -score. GO-CBED performs better or comparatively in terms of uncertainty reduction ( $\mathcal{R}_{T;L}$ ), structural recovery ( $\mathbb{E}$ -SHD), and structural accuracy ( $F_1$ -score) compared to all baselines. Shaded regions indicate  $\pm 1$  standard error across 10 random seeds.

consider synthetic settings using ER and SF graph priors, and semi-synthetic settings based on real gene regulatory networks from DREAM [27]. In all cases, we simulate linear and nonlinear causal mechanisms with additive noise. See Appendix C.3 for more details.

**Baselines** We benchmark GO-CBED against four methods: **CAASL** [3], which uses offline RL method with a fixed pre-trained posterior network; **Random**, which uniformly selects interventions at random; **Soft-CBED** [61], which employs Bayesian optimization for single-step EIG; and **DiffCBED** [60], which learns a non-adaptive policy through gradient-based optimization.

**Metrics** We evaluate performance using three metrics: prior-omitted EIG lower bound  $\mathcal{R}_{T;L}$ ; expected structural Hamming distance  $\mathbb{E}$ -SHD [17] between posterior graph samples and the ground truth; and  $F_1$ -score for edge prediction. To ensure a fair comparison across policies, we train a dedicated posterior network for each policy. This isolates the contribution of the policy itself and avoids confounding effects from differing posterior approximation methods. For example, while CAASL relies on a fixed pre-trained posterior network from [41], other baselines use DAG-bootstrap [21, 29] for linear SCMs and DiBS [40] for nonlinear SCMs. In our evaluation, we adopt the specifically trained posterior networks for inference across all baselines, as they produce higher-quality posteriors than those used in the original works. For completeness, results using each method’s original inference setup are included in Appendix D.3. All results are averaged over 10 random seeds.

**Synthetic SCMs** Figure 5 presents GO-CBED’s performance using ER and SF graph priors with linear ( $d = 30, T = 15$ ) and nonlinear ( $d = 20, T = 10$ ) mechanisms. Across all metrics and graph types, GO-CBED consistently outperforms baseline methods, showing especially large gains

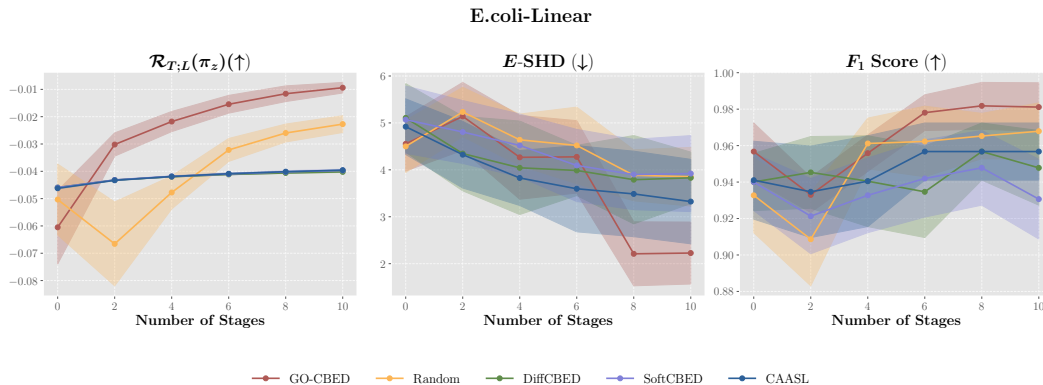


Figure 6: GO-CBED outperforms all baselines on semi-synthetic *E. coli* gene regulatory networks ( $d = 20, T = 10$ ) with linear mechanisms. Our method achieves: (*Left*) near-zero  $\mathcal{R}_{T;L}(\pi_z; \lambda, \phi)$ , (*Middle*) significant lower  $\mathbb{E}\text{-SHD}$ , and (*Right*) superior  $F_1$  score for edge prediction. This demonstrates GO-CBED’s ability to efficiently identify the true causal structure in biologically-inspired networks, with the variational posterior tightly concentrated around the ground truth after 10 stages.

in  $F_1$ -scores (reaching up to 0.75 on SF graphs). Although GO-CBED initially performs comparably to some baselines, it steadily surpasses them as more interventions are collected. This highlights its strength in optimizing long-term information gain rather than short-term or greedy improvements. While the advantage is most prominent in linear settings, GO-CBED still achieves strong performance in the more challenging nonlinear cases. We further evaluate GO-CBED’s robustness to distributional shifts in observation noise with additional experiments in Appendix D.5.

**Semi-Synthetic Gene Regulatory Networks** Figure 6 evaluates GO-CBED on 20-node networks derived from the DREAM *E. coli* gene regulatory benchmark with linear mechanisms. Our method consistently outperforms all baselines across all evaluation metrics. By the final intervention stage, GO-CBED achieves high  $\mathcal{R}_{T;L}$  values, low  $\mathbb{E}\text{-SHD}$  scores, and high  $F_1$ -scores, indicating accurate recovery of the true causal structure with minimal posterior uncertainty. This strong performance on biologically-inspired networks demonstrates GO-CBED’s ability to handle the complex dependencies and noise typically encountered in gene regulatory systems. Additional experiments on Yeast networks and with nonlinear mechanisms presented in Appendix D.4 further support GO-CBED’s effectiveness in biologically relevant settings.

## 6 Discussion

We presented GO-CBED, a goal-oriented Bayesian framework for sequential causal experimental design. Unlike conventional approaches that aim to learn the full causal model, GO-CBED directly maximizes the EIG on specific causal QoIs, enabling more targeted and efficient experimentation. The framework is both non-myopic, optimizing over entire sequences of interventions, and goal-oriented, focusing on model aspects relevant to the causal query. To overcome the intractability of exact EIG computation, we introduced a variational lower bound, optimized jointly over policy and variational parameters. Our implementation leveraged NFs for flexible posterior approximations and a transformer-based policy network that captures symmetry and structure in the intervention history. Numerical experiments demonstrated that GO-CBED outperforms baseline methods in multiple causal tasks, with gains increasing as causal mechanisms become more complex. Crucially, the joint training of intervention policies and variational posteriors enabled adaptive, goal-oriented exploration of the causal model.

**Limitations and Future Work** While GO-CBED demonstrates strong empirical performance, several limitations remain. Its scalability is constrained by the complexity of both the underlying causal models and the neural network architectures. Additionally, its effectiveness depends on the availability of prior knowledge over causal structures and mechanisms. Future work includes incorporating foundation models as high-fidelity world simulators for offline policy training. Recent advances

in biological foundation models [59, 15] offer a promising avenue for simulating complex, realistic causal mechanisms, which could significantly enhance policy learning without relying on costly real-world experimentation. Other valuable extensions include generalizing GO-CBED to support multi-target intervention settings and non-differentiable likelihoods, as well as improving policy robustness to changing experimental horizons and dynamic model updates during experimentation.

## References

- [1] Agrawal, R., Squires, C., Yang, K., Shanmugam, K., and Uhler, C. (2019). Abcd-strategy: Budgeted experimental design for targeted causal structure discovery. In *The 22nd International Conference on Artificial Intelligence and Statistics*, pages 3400–3409. PMLR.
- [2] Annadani, Y., Rothfuss, J., Lacoste, A., Scherrer, N., Goyal, A., Bengio, Y., and Bauer, S. (2021). Variational causal networks: Approximate bayesian inference over causal structures. *arXiv preprint arXiv:2106.07635*.
- [3] Annadani, Y., Tigas, P., Bauer, S., and Foster, A. (2024). Amortized active causal induction with deep reinforcement learning. *arXiv preprint arXiv:2405.16718*.
- [4] Atkinson, A. C., Donev, A. N., and Tobias, R. D. (2007). *Optimum Experimental Designs, With SAS*. Oxford University Press.
- [5] Attia, A., Alexanderian, A., and Saibaba, A. K. (2018). Goal-oriented optimal design of experiments for large-scale Bayesian linear inverse problems. *Inverse Problems*, 34(9):095009.
- [6] Barabási, A.-L. and Albert, R. (1999). Emergence of scaling in random networks. *Science*, 286(5439):509–512.
- [7] Barber, D. and Agakov, F. (2004). The IM algorithm: a variational approach to information maximization. *Advances in Neural Information Processing Systems*, 16(320):201.
- [8] Bernardo, J. M. (1979). Expected Information as Expected Utility. *The Annals of Statistics*, 7(3):686–690.
- [9] Bingham, E., Chen, J. P., Jankowiak, M., Obermeyer, F., Pradhan, N., Karaletsos, T., Singh, R., Szerlip, P., Horsfall, P., and Goodman, N. D. (2019). Pyro: Deep universal probabilistic programming. *Journal of Machine Learning Research*, 20(28):1–6.
- [10] Blau, T., Bonilla, E. V., Chades, I., and Dezfouli, A. (2022). Optimizing sequential experimental design with deep reinforcement learning. In *International Conference on Machine Learning*, pages 2107–2128. PMLR.
- [11] Brouillard, P., Lachapelle, S., Lacoste, A., Lacoste-Julien, S., and Drouin, A. (2020). Differentiable causal discovery from interventional data. *Advances in Neural Information Processing Systems*, 33:21865–21877.
- [12] Chakraborty, A., Huan, X., and Catanach, T. (2024). A likelihood-free approach to goal-oriented Bayesian optimal experimental design. *arXiv preprint arXiv:2408.09582*.
- [13] Chaloner, K. and Verdinelli, I. (1995). Bayesian Experimental Design: A Review. *Statistical Science*, 10(3):273 – 304.
- [14] Cho, H., Berger, B., and Peng, J. (2016). Reconstructing causal biological networks through active learning. *PloS One*, 11(3):e0150611.
- [15] Cui, H., Wang, C., Maan, H., Pang, K., Luo, F., Duan, N., and Wang, B. (2024). scGPT: toward building a foundation model for single-cell multi-omics using generative AI. *Nature Methods*, pages 1–11.
- [16] Cundy, C., Grover, A., and Ermon, S. (2021). Bcd nets: Scalable variational approaches for bayesian causal discovery. *Advances in Neural Information Processing Systems*, 34:7095–7110.

- [17] de Jongh, M. and Druzdzel, M. J. (2009). A comparison of structural distance measures for causal Bayesian network models. Recent Advances in Intelligent Information Systems, Challenging Problems of Science, Computer Science Series, pages 443–456.
- [18] Dinh, L., Sohl-Dickstein, J., and Bengio, S. (2016). Density estimation using real nvp. arXiv preprint arXiv:1605.08803.
- [19] Dong, J., Jacobsen, C., Khalloufi, M., Akram, M., Liu, W., Duraisamy, K., and Huan, X. (2025). Variational Bayesian optimal experimental design with normalizing flows. Computer Methods in Applied Mechanics and Engineering, 433.
- [20] Foster, A., Ivanova, D. R., Malik, I., and Rainforth, T. (2021). Deep adaptive design: Amortizing sequential Bayesian experimental design. In International Conference on Machine Learning, pages 3384–3395. PMLR.
- [21] Friedman, N., Goldszmidt, M., and Wyner, A. (2013). Data analysis with Bayesian networks: A bootstrap approach. arXiv preprint arXiv:1301.6695.
- [22] Friedman, N. and Koller, D. (2003). Being Bayesian about network structure: A Bayesian approach to structure discovery in Bayesian networks. Machine Learning, 50:95–125.
- [23] Gamella, J. L. and Heinze-Deml, C. (2020). Active invariant causal prediction: Experiment selection through stability. Advances in Neural Information Processing Systems, 33:15464–15475.
- [24] Gao, H., Sun, Z., Yang, H., and Chen, X. (2024). Policy-based bayesian active causal discovery with deep reinforcement learning. In Proceedings of the 30th ACM SIGKDD Conference on Knowledge Discovery and Data Mining, pages 839–850.
- [25] Ghassami, A., Salehkaleybar, S., Kiyavash, N., and Bareinboim, E. (2018). Budgeted experiment design for causal structure learning. In International Conference on Machine Learning, pages 1724–1733. PMLR.
- [26] Glymour, C., Zhang, K., and Spirtes, P. (2019). Review of causal discovery methods based on graphical models. Frontiers in Genetics, 10:524.
- [27] Greenfield, A., Madar, A., Ostrer, H., and Bonneau, R. (2010). DREAM4: Combining genetic and dynamic information to identify biological networks and dynamical models. PloS one, 5(10):e13397.
- [28] Hagberg, A., Swart, P., and S Chult, D. (2008). Exploring network structure, dynamics, and function using networkx. Technical report, Los Alamos National Lab.(LANL), Los Alamos, NM (United States).
- [29] Hauser, A. and Bühlmann, P. (2012). Characterization and greedy learning of interventional Markov equivalence classes of directed acyclic graphs. The Journal of Machine Learning Research, 13(1):2409–2464.
- [30] Heckerman, D., Meek, C., and Cooper, G. (2006). A Bayesian approach to causal discovery. Innovations in Machine Learning: Theory and Applications, pages 1–28.
- [31] Heinze-Deml, C., Maathuis, M. H., and Meinshausen, N. (2018). Causal structure learning. Annual Review of Statistics and Its Application, 5:371–391.
- [32] Huan, X., Jagalur, J., and Marzouk, Y. (2024). Optimal experimental design: Formulations and computations. Acta Numerica, 33:715–840.
- [33] Imbens, G. W. (2024). Causal inference in the social sciences. Annual Review of Statistics and Its Application, 11.
- [34] Ivanova, D. R., Foster, A., Kleinegesse, S., Gutmann, M. U., and Rainforth, T. (2021). Implicit deep adaptive design: policy-based experimental design without likelihoods. Advances in Neural Information Processing Systems, 34:25785–25798.
- [35] Kocaoglu, M., Dimakis, A., and Vishwanath, S. (2017a). Cost-optimal learning of causal graphs. In International Conference on Machine Learning, pages 1875–1884. PMLR.

- [36] Kocaoglu, M., Shanmugam, K., and Bareinboim, E. (2017b). Experimental design for learning causal graphs with latent variables. Advances in Neural Information Processing Systems, 30.
- [37] Lindley, D. V. (1956). On a measure of the information provided by an experiment. The Annals of Mathematical Statistics, 27(4):986–1005.
- [38] Lippe, P., Cohen, T., and Gavves, E. (2021). Efficient neural causal discovery without acyclicity constraints. arXiv preprint arXiv:2107.10483.
- [39] Liu, Q. and Wang, D. (2016). Stein variational gradient descent: A general purpose Bayesian inference algorithm. Advances in Neural Information Processing Systems, 29.
- [40] Lorch, L., Rothfuss, J., Schölkopf, B., and Krause, A. (2021). Dibs: Differentiable bayesian structure learning. Advances in Neural Information Processing Systems, 34:24111–24123.
- [41] Lorch, L., Sussex, S., Rothfuss, J., Krause, A., and Schölkopf, B. (2022). Amortized inference for causal structure learning. Advances in Neural Information Processing Systems, 35:13104–13118.
- [42] Mokhtarian, E., Salehkaleybar, S., Ghassami, A., and Kiyavash, N. (2022). A unified experiment design approach for cyclic and acyclic causal models. arXiv preprint arXiv:2205.10083.
- [43] Murphy, K. P. (2001). Active learning of causal bayes net structure. Technical report, technical report, UC Berkeley.
- [44] Ness, R. O., Sachs, K., Mallick, P., and Vitek, O. (2018). A Bayesian active learning experimental design for inferring signaling networks. Journal of Computational Biology, 25(7):709–725.
- [45] Olko, M., Zając, M., Nowak, A., Scherrer, N., Annadani, Y., Bauer, S., Kuciński, Ł., and Miłoś, P. (2024). Trust your  $\nabla$ : Gradient-based intervention targeting for causal discovery. Advances in Neural Information Processing Systems, 36.
- [46] Pearl, J. (2009). Causality. Cambridge University Press.
- [47] Perry, R., Von Kügelgen, J., and Schölkopf, B. (2022). Causal discovery in heterogeneous environments under the sparse mechanism shift hypothesis. Advances in Neural Information Processing Systems, 35:10904–10917.
- [48] Peters, J., Bühlmann, P., and Meinshausen, N. (2016). Causal inference by using invariant prediction: identification and confidence intervals. Journal of the Royal Statistical Society Series B: Statistical Methodology, 78(5):947–1012.
- [49] Peters, J., Janzing, D., and Schölkopf, B. (2017). Elements of causal inference: foundations and learning algorithms. The MIT Press.
- [50] Poole, B., Ozair, S., Van Den Oord, A., Alemi, A., and Tucker, G. (2019). On variational bounds of mutual information. In Proceedings of the 36th International Conference on Machine Learning (ICML 2019), volume 97 of Proceedings of Machine Learning Research, pages 5171–5180. PMLR.
- [51] Rainforth, T., Foster, A., Ivanova, D. R., and Bickford Smith, F. (2024). Modern Bayesian experimental design. Statistical Science, 39(1):100–114.
- [52] Shen, W., Dong, J., and Huan, X. (2025). Variational sequential optimal experimental design using reinforcement learning. Computer Methods in Applied Mechanics and Engineering, (444):118068.
- [53] Shen, W. and Huan, X. (2023). Bayesian sequential optimal experimental design for nonlinear models using policy gradient reinforcement learning. Computer Methods in Applied Mechanics and Engineering, 416:116304.
- [54] Smith, F. B., Kirsch, A., Farquhar, S., Gal, Y., Foster, A., and Rainforth, T. (2023). Prediction-oriented Bayesian active learning. In International Conference on Artificial Intelligence and Statistics, pages 7331–7348. PMLR.

- [55] Sobel, M. E. (2000). Causal inference in the social sciences. Journal of the American Statistical Association, 95(450):647–651.
- [56] Spirtes, P., Glymour, C. N., and Scheines, R. (2000). Causation, Prediction, and Search. The MIT press.
- [57] Sussex, S., Uhler, C., and Krause, A. (2021). Near-optimal multi-perturbation experimental design for causal structure learning. Advances in Neural Information Processing Systems, 34:777–788.
- [58] Tejada-Lapuerta, A., Bertin, P., Bauer, S., Aliee, H., Bengio, Y., and Theis, F. J. (2023). Causal machine learning for single-cell genomics. arXiv preprint arXiv:2310.14935.
- [59] Theodoris, C. V., Xiao, L., Chopra, A., Chaffin, M. D., Al Sayed, Z. R., Hill, M. C., Mantineo, H., Brydon, E. M., Zeng, Z., Liu, X. S., et al. (2023). Transfer learning enables predictions in network biology. Nature, 618(7965):616–624.
- [60] Tigas, P., Annadani, Y., Ivanova, D. R., Jesson, A., Gal, Y., Foster, A., and Bauer, S. (2023). Differentiable multi-target causal Bayesian experimental design. In International Conference on Machine Learning, pages 34263–34279. PMLR.
- [61] Tigas, P., Annadani, Y., Jesson, A., Schölkopf, B., Gal, Y., and Bauer, S. (2022). Interventions, where and how? Experimental design for causal models at scale. Advances in Neural Information Processing Systems, 35:24130–24143.
- [62] Tong, S. and Koller, D. (2001). Active learning for structure in Bayesian networks. In International Joint Conference on Artificial Intelligence, volume 17, pages 863–869.
- [63] Toth, C., Lorch, L., Knoll, C., Krause, A., Pernkopf, F., Peharz, R., and Von Kügelgen, J. (2022). Active Bayesian causal inference. Advances in Neural Information Processing Systems, 35:16261–16275.
- [64] Varian, H. R. (2016). Causal inference in economics and marketing. Proceedings of the National Academy of Sciences, 113(27):7310–7315.
- [65] Verma, T. S. and Pearl, J. (2022). Equivalence and synthesis of causal models. In Probabilistic and Causal Inference: The works of Judea Pearl, pages 221–236.
- [66] von Kügelgen, J., Rubenstein, P. K., Schölkopf, B., and Weller, A. (2019). Optimal experimental design via Bayesian optimization: active causal structure learning for gaussian process networks. arXiv preprint arXiv:1910.03962.
- [67] Vowels, M. J., Camgoz, N. C., and Bowden, R. (2022). D’ya like dags? a survey on structure learning and causal discovery. ACM Computing Surveys, 55(4):1–36.
- [68] Wu, K., Chen, P., and Ghattas, O. (2021). An efficient method for goal-oriented linear Bayesian optimal experimental design: Application to optimal sensor placement. arXiv preprint arXiv:2102.06627.
- [69] Zhong, S., Shen, W., Catanach, T., and Huan, X. (2024). Goal-oriented Bayesian optimal experimental design for nonlinear models using Markov chain Monte Carlo. arXiv preprint arXiv:2403.18072.

## Appendix

<b>A</b>	<b>Theoretical and Numerical Formulations</b>	<b>15</b>
A.1	Incremental EIG Formulation . . . . .	15
A.2	Proof for Theorem 4.1 . . . . .	16
A.3	Prior-omitted EIG . . . . .	16
A.4	Normalizing Flows . . . . .	17
<b>B</b>	<b>Detailed Related Work</b>	<b>17</b>
<b>C</b>	<b>Experiment Details</b>	<b>18</b>
C.1	Hyperparameter Settings For Policy and Posterior Networks . . . . .	18
C.2	Example in Section 5.1 . . . . .	20
C.3	Examples in Sections 5.2 and 5.3 . . . . .	21
C.4	Incorporating Existing Observational Data into the Prior . . . . .	22
<b>D</b>	<b>Additional Experiments</b>	<b>23</b>
D.1	Higher Bias in the NMC Estimator . . . . .	23
D.2	Causal Reasoning on Diverse Realistic Graph Structures . . . . .	23
D.3	Performance Comparison with Original Posterior Inference Methods . . . . .	24
D.4	Extended Evaluation on Causal Discovery Tasks . . . . .	25
D.5	Distributional Shift in Observation Noise . . . . .	28

## A Theoretical and Numerical Formulations

### A.1 Incremental EIG Formulation

The incremental EIG on the target query  $\mathbf{z}$  resulting from an experiment at stage  $t$  with design  $\xi_t$ , given the intervention history  $\mathbf{h}_{t-1}$ , is defined as:

$$\mathcal{I}_t(\xi_t, \mathbf{h}_{t-1}) := \mathbb{E}_{p(\mathcal{M}|\mathbf{h}_{t-1})p(\mathbf{x}_t|\mathcal{M},\xi_t)p(\mathbf{z}|\mathcal{M})} \left[ \log \frac{p(\mathbf{z}|\mathbf{h}_t)}{p(\mathbf{z}|\mathbf{h}_{t-1})} \right]. \quad (\text{A1})$$

**Proposition A.1.** *The total EIG of a policy  $\pi$  on the target query  $\mathbf{z}$  over a sequence of  $T$  experiments can be written as:*

$$\mathcal{I}_T(\pi) = \mathbb{E}_{p(\mathbf{h}_T|\pi)} \left[ \sum_{t=1}^T \mathcal{I}_t(\xi_t, \mathbf{h}_{t-1}) \right]. \quad (\text{A2})$$

*Proof.* Beginning from the right-hand side, we have:

$$\begin{aligned} & \mathbb{E}_{p(\mathbf{h}_T|\pi)} \left[ \sum_{t=1}^T \mathcal{I}_t(\xi_t, \mathbf{h}_{t-1}) \right] \\ &= \mathbb{E}_{p(\mathbf{h}_T|\pi)} \left[ \sum_{t=1}^T \mathbb{E}_{p(\mathcal{M}|\mathbf{h}_{t-1})p(\mathbf{x}_t|\mathcal{M},\xi_t)p(\mathbf{z}|\mathcal{M})} \left[ \log \frac{p(\mathbf{z}|\mathbf{h}_t)}{p(\mathbf{z}|\mathbf{h}_{t-1})} \right] \right] \\ &= \sum_{t=1}^T \left[ \mathbb{E}_{p(\mathbf{h}_{t-1}|\pi)} \left[ \mathbb{E}_{p(\mathcal{M}|\mathbf{h}_{t-1})p(\mathbf{x}_t|\mathcal{M},\xi_t)p(\mathbf{z}|\mathcal{M})} \left[ \log \frac{p(\mathbf{z}|\mathbf{h}_t)}{p(\mathbf{z}|\mathbf{h}_{t-1})} \right] \right] \right] \\ &= \sum_{t=1}^T \left[ \mathbb{E}_{p(\mathcal{M},\mathbf{x}_t,\mathbf{h}_{t-1},\mathbf{z}|\pi)} \left[ \log \frac{p(\mathbf{z}|\mathbf{h}_t)}{p(\mathbf{z}|\mathbf{h}_{t-1})} \right] \right] \\ &= \sum_{t=1}^T \left[ \mathbb{E}_{p(\mathcal{M},\mathbf{h}_t|\pi)p(\mathbf{z}|\mathcal{M})} \log p(\mathbf{z}|\mathbf{h}_t) - \mathbb{E}_{p(\mathcal{M},\mathbf{h}_{t-1}|\pi)p(\mathbf{z}|\mathcal{M})} \log p(\mathbf{z}|\mathbf{h}_{t-1}) \right] \\ &= \mathbb{E}_{p(\mathcal{M},\mathbf{h}_T|\pi)p(\mathbf{z}|\mathcal{M})} \left[ \log \frac{p(\mathbf{z}|\mathbf{h}_T)}{p(\mathbf{z})} \right] \\ &= \mathcal{I}_T(\pi), \end{aligned} \quad (\text{A3})$$

where in the third equality, the joint expectation is formed using  $p(\mathbf{z}|\mathcal{M}) = p(\mathbf{z}|\mathcal{M}, \mathbf{h}_{t-1})$ , and the fifth equality follows from the cancellation of all terms in the summation except the first and last.  $\square$

## A.2 Proof for Theorem 4.1

*Proof for Theorem 4.1.* Following (4) and (5), the difference

$$\begin{aligned}
& \mathcal{I}_T(\pi) - \mathcal{I}_{T;L}(\pi; \boldsymbol{\lambda}, \boldsymbol{\phi}) \\
&= \mathbb{E}_{p(\mathcal{M})p(\mathbf{h}_T|\mathcal{M},\pi)p(\mathbf{z}|\mathcal{M})} \left[ \log \frac{p(\mathbf{z}|\mathbf{h}_T)}{p(\mathbf{z})} \right] - \mathbb{E}_{p(\mathcal{M})p(\mathbf{h}_T|\mathcal{M},\pi)p(\mathbf{z}|\mathcal{M})} \left[ \log \frac{q_{\boldsymbol{\lambda}}(\mathbf{z}|f_{\boldsymbol{\phi}}(\mathbf{h}_T))}{p(\mathbf{z})} \right] \\
&= \mathbb{E}_{p(\mathcal{M})p(\mathbf{h}_T|\mathcal{M},\pi)p(\mathbf{z}|\mathcal{M})} \left[ \log \frac{p(\mathbf{z}|\mathbf{h}_T)}{q_{\boldsymbol{\lambda}}(\mathbf{z}|f_{\boldsymbol{\phi}}(\mathbf{h}_T))} \right] \\
&= \mathbb{E}_{p(\mathcal{M},\mathbf{h}_T,\mathbf{z}|\pi)} \left[ \log \frac{p(\mathbf{z}|\mathbf{h}_T)}{q_{\boldsymbol{\lambda}}(\mathbf{z}|f_{\boldsymbol{\phi}}(\mathbf{h}_T))} \right] \\
&= \mathbb{E}_{p(\mathbf{h}_T,\mathbf{z}|\pi)} \left[ \log \frac{p(\mathbf{z}|\mathbf{h}_T)}{q_{\boldsymbol{\lambda}}(\mathbf{z}|f_{\boldsymbol{\phi}}(\mathbf{h}_T))} \right] \\
&= \mathbb{E}_{p(\mathbf{h}_T|\pi)p(\mathbf{z}|\mathbf{h}_T)} \left[ \log \frac{p(\mathbf{z}|\mathbf{h}_T)}{q_{\boldsymbol{\lambda}}(\mathbf{z}|f_{\boldsymbol{\phi}}(\mathbf{h}_T))} \right] \\
&= \mathbb{E}_{p(\mathbf{h}_T|\pi)} \left[ D_{\text{KL}} \left( p(\mathbf{z}|\mathbf{h}_T) \parallel q_{\boldsymbol{\lambda}}(\mathbf{z}|f_{\boldsymbol{\phi}}(\mathbf{h}_T)) \right) \right] \tag{A4}
\end{aligned}$$

is an expectation of a Kullback–Leibler (KL) divergence, which is always non-negative. Hence,  $\mathcal{I}_T(\pi) \geq \mathcal{I}_{T;L}(\pi; \boldsymbol{\lambda}, \boldsymbol{\phi})$  for any  $\pi$ ,  $\boldsymbol{\lambda}$ , and  $\boldsymbol{\phi}$ . The bound is tight if and only if the KL divergence equals zero, which occurs when  $q_{\boldsymbol{\lambda}}(\mathbf{z}|f_{\boldsymbol{\phi}}(\mathbf{h}_T)) = p(\mathbf{z}|\mathbf{h}_T)$  for all  $\mathbf{z}$  and  $\mathbf{h}_T$ .  $\square$

## A.3 Prior-omitted EIG

We note that

$$\begin{aligned}
\mathcal{I}_T(\pi) &= \mathbb{E}_{p(\mathcal{M})p(\mathbf{h}_T|\mathcal{M},\pi)p(\mathbf{z}|\mathcal{M})} [\log p(\mathbf{z}|\mathbf{h}_T)] - c \\
&= \mathcal{R}_T(\pi) - c, \tag{A5}
\end{aligned}$$

where  $c := \mathbb{E}_{p(\mathcal{M})p(\mathbf{z}|\mathcal{M})} [\log p(\mathbf{z})]$  is independent of  $\pi$ . Similarly,

$$\begin{aligned}
\mathcal{I}_{T;L}(\pi; \boldsymbol{\lambda}, \boldsymbol{\phi}) &= \mathbb{E}_{p(\mathcal{M})p(\mathbf{h}_T|\mathcal{M},\pi)p(\mathbf{z}|\mathcal{M})} [\log q_{\boldsymbol{\lambda}}(\mathbf{z}|f_{\boldsymbol{\phi}}(\mathbf{h}_T))] - c \\
&= \mathcal{R}_{T;L}(\pi; \boldsymbol{\lambda}, \boldsymbol{\phi}) - c. \tag{A6}
\end{aligned}$$

**Proposition A.2.** *For any policy  $\pi$ , variational parameter  $\boldsymbol{\lambda}$ , and embedding parameter  $\boldsymbol{\phi}$ , the prior-omitted EIG satisfies  $\mathcal{R}_T(\pi) \geq \mathcal{R}_{T;L}(\pi; \boldsymbol{\lambda}, \boldsymbol{\phi})$ . The bound is tight if and only if  $p(\mathbf{z}|\mathbf{h}_T) = q_{\boldsymbol{\lambda}}(\mathbf{z}|f_{\boldsymbol{\phi}}(\mathbf{h}_T))$  for all  $\mathbf{z}$  and  $\mathbf{h}_T$ .*

*Proof.*  $\mathcal{R}_T(\pi) = \mathcal{I}_T(\pi) + c \geq \mathcal{I}_{T;L}(\pi; \boldsymbol{\lambda}, \boldsymbol{\phi}) + c = \mathcal{R}_{T;L}(\pi; \boldsymbol{\lambda}, \boldsymbol{\phi})$ , making use of  $\mathcal{I}_T(\pi) \geq \mathcal{I}_{T;L}(\pi; \boldsymbol{\lambda}, \boldsymbol{\phi})$  from Theorem 4.1.  $\square$

We adopt standard Monte Carlo to estimate  $\mathcal{R}_{T;L}(\pi; \boldsymbol{\lambda}, \boldsymbol{\phi})$ :

$$\begin{aligned}
\mathcal{R}_{T;L}(\pi; \boldsymbol{\lambda}, \boldsymbol{\phi}) &= \mathbb{E}_{p(\mathcal{M})p(\mathbf{h}_T|\mathcal{M},\pi)p(\mathbf{z}|\mathcal{M})} [\log q_{\boldsymbol{\lambda}}(\mathbf{z}|f_{\boldsymbol{\phi}}(\mathbf{h}_T))] \\
&\approx \frac{1}{N} \sum_{i=1}^N \log q_{\boldsymbol{\lambda}}(\mathbf{z}^i|f_{\boldsymbol{\phi}}(\mathbf{h}_T^i)), \tag{A7}
\end{aligned}$$

where  $\mathcal{M}^i \sim p(\mathcal{M})$ ,  $\mathbf{h}_T^i \sim p(\mathbf{h}_T|\mathcal{M}^i, \pi)$ , and  $\mathbf{z}^i \sim p(\mathbf{z}|\mathcal{M}^i)$ .

We further propose a NMC estimator to estimate  $\mathcal{R}_T(\pi)$ :

$$\begin{aligned}
\mathcal{R}_T(\pi) &= \mathbb{E}_{p(\mathcal{M})p(\mathbf{h}_T|\mathcal{M},\pi)p(\mathbf{z}|\mathcal{M})} [\log p(\mathbf{z}|\mathbf{h}_T)] \\
&= \mathbb{E}_{p(\mathcal{M})p(\mathbf{h}_T|\mathcal{M},\pi)p(\mathbf{z}|\mathcal{M})} [\log p(\mathbf{z}, \mathbf{h}_T|\pi) - \log p(\mathbf{h}_T|\pi)] \\
&= \mathbb{E}_{p(\mathcal{M})p(\mathbf{h}_T|\mathcal{M},\pi)p(\mathbf{z}|\mathcal{M})} [\log \mathbb{E}_{p(\mathcal{M}')} [p(\mathbf{z}, \mathbf{h}_T|\mathcal{M}', \pi)] - \log \mathbb{E}_{p(\mathcal{M}'')} [p(\mathbf{h}_T|\mathcal{M}'', \pi)]] \\
&\approx \frac{1}{N} \sum_{i=1}^N \left[ \log \frac{1}{M_1} \sum_{j_1=1}^{M_1} p(\mathbf{z}^i, \mathbf{h}_T^i|\mathcal{M}^{j_1}, \pi) - \log \frac{1}{M_2} \sum_{j_2=1}^{M_2} p(\mathbf{h}_T^i|\mathcal{M}^{j_2}, \pi) \right], \tag{A8}
\end{aligned}$$

where  $\mathcal{M}^i \sim p(\mathcal{M})$ ,  $\mathbf{h}_T^i \sim p(\mathbf{h}_T|\mathcal{M}^i, \pi)$ ,  $\mathbf{z}^i \sim p(\mathbf{z}|\mathcal{M}^i)$ , and  $\mathcal{M}^{j_1} \sim p(\mathcal{M}')$  and  $\mathcal{M}^{j_2} \sim p(\mathcal{M}'')$ . This NMC estimator is only used in Section 5.1 as a baseline comparison.

#### A.4 Normalizing Flows

An NF is an invertible transformation that maps a target random variable  $\mathbf{z}$  to a standard normal random variable  $\boldsymbol{\eta}$ , such that  $\mathbf{z} = g(\boldsymbol{\eta})$  and  $\boldsymbol{\eta} = f(\mathbf{z})$ , where  $f = g^{-1}$ . The probability densities of  $\mathbf{z}$  and  $\boldsymbol{\eta}$  are related via the change-of-variables formula:

$$p(\mathbf{z}) = p_{\boldsymbol{\eta}}(f(\mathbf{z})) \left| \det \frac{\partial f(\mathbf{z})}{\partial \mathbf{z}} \right|. \tag{A9}$$

Let the transformation  $g$  be expressed as a composition of  $n \geq 1$  successive invertible functions:  $\mathbf{z} = g(\boldsymbol{\eta}) = g_1 \circ g_2 \circ \dots \circ g_n(\boldsymbol{\eta}) = g_1(g_2(\dots(g_n(\boldsymbol{\eta}))\dots))$ . Then, the corresponding log-density of  $\mathbf{z}$  becomes:

$$\log p(\mathbf{z}) = \log p_{\boldsymbol{\eta}}(f_n \circ f_{n-1} \circ \dots \circ f_1(\mathbf{z})) + \sum_{i=1}^n \log \left| \det \frac{\partial f_i \circ f_{i-1} \circ \dots \circ f_1(\mathbf{z})}{\partial \mathbf{z}} \right|, \tag{A10}$$

where  $\boldsymbol{\eta} = f(\mathbf{z}) = f_n \circ f_{n-1} \circ \dots \circ f_1(\mathbf{z})$  and  $f_i = g_i^{-1}$ . Through these successive transformations, NFs can model highly expressive and flexible densities for the target variable  $\mathbf{z}$  [18].

To approximate the QoI posterior  $q_{\lambda}(\mathbf{z}|f_{\phi}(\mathbf{h}_T))$ , we employ NFs composed of successive coupling layers. Each coupling layer partitions  $\mathbf{z}$  into two similarly sized subsets,  $\mathbf{z} = [\mathbf{z}_1, \mathbf{z}_2]^{\top}$ , with dimensions  $n_{z_1}$  and  $n_{z_2}$ , respectively. The coupling transformations are defined as:

$$\begin{aligned}
f_1(\mathbf{z}) &= \begin{pmatrix} \mathbf{z}_1 \\ \tilde{\mathbf{z}}_2 := \mathbf{z}_2 \odot \exp(s_1(\mathbf{z}_1)) + t_1(\mathbf{z}_1) \end{pmatrix} \\
f_2(f_1(\mathbf{z})) &= \begin{pmatrix} \tilde{\mathbf{z}}_1 := \mathbf{z}_1 \odot \exp(s_2(\tilde{\mathbf{z}}_2)) + t_2(\tilde{\mathbf{z}}_2) \\ \tilde{\mathbf{z}}_2 \end{pmatrix}, \tag{A11}
\end{aligned}$$

where  $s_1, t_1 : \mathbb{R}^{n_{z_1}} \mapsto \mathbb{R}^{n_{z_2}}$  and  $s_2, t_2 : \mathbb{R}^{n_{z_2}} \mapsto \mathbb{R}^{n_{z_1}}$  are flexible mappings (e.g., neural networks), and  $\odot$  denotes the element-wise product. The Jacobian of the transformation  $f_1$  is given by:

$$\begin{bmatrix} \mathbb{I}_d & 0 \\ \frac{\partial f_1(\mathbf{z})}{\partial \mathbf{z}_2} & \text{diag}(\exp(s_1(\mathbf{z}_1))) \end{bmatrix},$$

which is lower-triangular with determinant  $\exp(\sum_{j=1}^{n_{z_2}} s_1(\mathbf{z}_1)_j)$ . Similarly, the Jacobian of  $f_2$  is upper-triangular with determinant  $\exp(\sum_{j=1}^{n_{z_1}} s_2(\tilde{\mathbf{z}}_2)_j)$ . Multiple coupling transformations ( $n_{\text{trans}}$ ) from (A11) can be composed sequentially to increase the expressive power of the overall transformation. To capture the dependencies of the intervention history  $\mathbf{h}_T$ , we additionally condition the mappings  $s(\cdot)$  and  $t(\cdot)$  on the embedding  $f_{\phi}(\mathbf{h}_T)$ .

## B Detailed Related Work

Our work on GO-CBED builds upon several related lines of research.

**Causal Bayesian Experimental Design** Experimental design for causal discovery within a BOED framework was initially explored by Murphy [43] and Tong and Koller [62] for discrete variables with single-target acquisition. Subsequent research extended this approach to continuous variables within BOED [14, 1, 66] and alternative frameworks [35, 23, 25, 45]. Notable non-BOED methods include strategies for cyclic structures [42] and latent variables [36]. Within BOED, Tigas et al. [61] proposed selecting single target-state pairs via stochastic batch acquisition, later extending this to gradient-based optimization to multiple target-state pairs [60]. Sussex et al. [57] introduced a greedy method for selecting multi-target experiments without specifying intervention states. More recently, Annadani et al. [3] proposed an adaptive sequential experimental design method for causal structure learning, although their objective—minimizing graph prediction error—is different from traditional BOED. Gao et al. [24] developed a reinforcement learning method for sequential experimental design using Prior Contrastive Estimation [20] as a reward function; however, their approach relies on initial observational data and is computationally intensive. In contrast, our method uses direct policy optimization with differentiable rewards, enabling more efficient training without needing initial observational data.

**Bayesian Causal Discovery** Causal discovery has been extensively studied in machine learning and statistics [26, 31, 49, 67]. Traditional causal discovery methods typically infer a single causal graph from observational data [11, 29, 38, 47, 48, 31]. In contrast, Bayesian causal discovery [22, 30, 62] seeks to infer a posterior distribution over SCMs. Recent work [16, 40, 2] has introduced variational approximations of the DAG posterior, enabling representation of uncertainty by a full distribution rather than a point estimate. Addressing the discrete nature of DAGs—which prevents straightforward gradient-based optimization—Lorch et al. [40] used Stein variational gradient descent (SVGD) [39] in a continuous latent embedding space, enabling efficient Bayesian inference over DAG structures.

**Goal-Oriented BOED** Goal-oriented BOED extends classical optimal design principles—such as  $L$ -,  $D_A$ -,  $I$ -,  $V$ -, and  $G$ -optimality [4]—by shifting the objective from general parameter estimation to directly maximizing utility for specific, downstream QoIs. The concept of tailoring experiments for particular goals, especially in nonlinear settings, was formulated by Bernardo [8]. Recent work has primarily focused on addressing computational challenges associated with optimizing the EIG for QoIs [5, 68, 54, 69, 12]. For example, Attia et al. [5] introduced gradient-based optimization approaches for  $D_A$ - and  $L$ -optimal designs in linear models, while Wu et al. [68] developed scalable low-rank approximations for high-dimensional QoIs. In nonlinear scenarios, methods leveraging Markov chain Monte Carlo combined with kernel density estimation [69] and likelihood-free density-ratio estimation approaches [12] have been proposed. Although powerful for general predictive tasks, these methods typically do not accommodate the unique structure of causal queries derived from SCMs or the interventional nature inherent to causal experimentation.

**Non-Myopic Sequential BOED** Non-myopic sequential BOED addresses the limitations of greedy, single-step experimental strategies by planning optimal sequences of interventions. Such methods have been broadly explored in various general settings [20, 34, 10, 53], including goal-oriented extensions such as vsOED [52]. Within causal BOED specifically, non-myopic approaches have predominantly focused on causal discovery tasks aimed at learning the graph structures [3, 24]. Although active learning methods targeting specific causal reasoning queries have also been proposed [63], these typically employ myopic (single-step) intervention designs, thus limiting their ability to strategically plan for long-term gains.

## C Experiment Details

### C.1 Hyperparameter Settings For Policy and Posterior Networks

The input to the policy network has shape  $(n = n_{\text{int}} \times T, d, 2)$ , where the last dimension encodes the intervention data and binary intervention masks. The policy network architecture (see Figure 7) proceeds as follows:

1. The input is passed through a fully connected layer, transforming it to shape  $(n_{\text{int}} \times T, d, n_{\text{embedding}})$ .
2. The embedded representation is processed through  $L$  stacked Transformer layers. Each layer includes:

- Two multi-head self-attention sublayers, each preceded by layer normalization and followed by dropout.
- A feedforward fully-connected (FFN) sublayer, also preceded by layer normalization and followed by dropout.

Residual connections are applied after each sublayer. This output retains the shape  $(n_{\text{int}} \times T, d, n_{\text{embedding}})$ .

3. A max-pooling operation is applied across the  $n_{\text{int}} \times T$  dimension, yielding a compressed representation of shape  $(d, n_{\text{embedding}})$ .
4. The pooled representation is passed through:
  - A target prediction layer, followed by a Gumbel-softmax transformation with temperature  $\tau$ , producing a discrete intervention target vector.
  - A separate value layer, with final outputs scaled to fall within a specific range  $\min_{\text{val}}$  and  $\max_{\text{val}}$ .

The detailed implementation setup is provided in Table 1. The “step” associated with  $\tau$  refers to the current training step, and the values of  $T$ ,  $n_{\text{step}}$ , and  $n_{\text{envs}}$  per training step are kept to be the same as those used for training the posterior networks (see below).

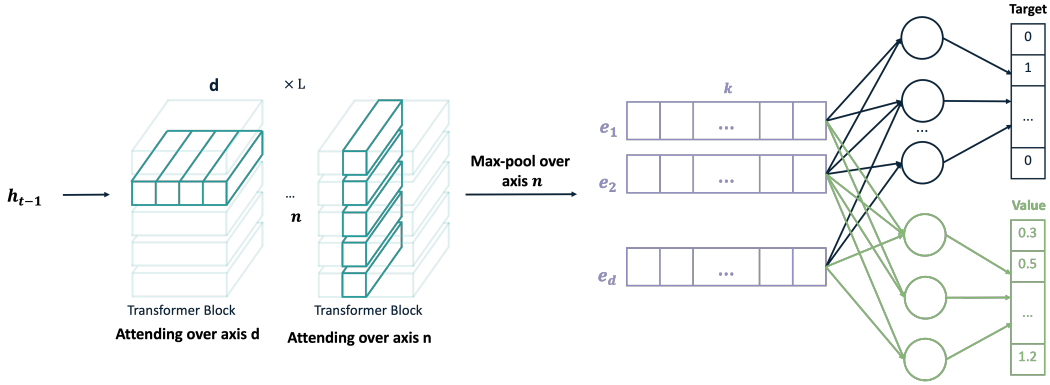


Figure 7: Policy network architecture. The model takes as input a three-dimensional tensor of shape  $n \times d \times 2$ , where  $n = n_{\text{int}} \times T$ . It is permutation-invariant along the  $n$ -axis and permutation-equivariant along the  $d$ -axis. Each of the  $L$  layers first applies self-attention across the  $d$ -axis, followed by attention across the  $n$ -axis, with shared parameters across the non-attended axis.

For the posterior networks, the initial input has shape  $(n_{\text{envs}}, n_{\text{int}} \times T, d, 2)$ , representing full trajectories. The processing steps follows the same as those of the policy network up to step 3, resulting in a max-pooled output of shape  $(n_{\text{envs}}, d, n_{\text{embedding}})$ . Specific to the causal discovery case, starting from step 4:

4. The pooled representation is processed as follows:
  - Two independent linear transformations are applied to produce vectors  $\mathbf{u}$  and  $\mathbf{v}$ , each of shape  $(n_{\text{envs}}, d, n_{\text{out}})$ .
  - Both  $\mathbf{u}$  and  $\mathbf{v}$  are normalized using their  $\ell_2$ -norm along the last dimension.
5. Pairwise edge logits are computed:
  - A dot product between every pair of variables  $\mathbf{u}_i$  and  $\mathbf{v}_j$ , resulting in a tensor of shape  $(n_{\text{envs}}, d, d)$ .
  - The logits are scaled by a learnable temperature parameter “temp” via the operation  $\text{logit}_{i,j} \times \exp(\text{temp})$ , which is then added element-wise with a learnable term, “bias”.

The detailed implementation setup is provided in Table 2.

Specific to the causal reasoning case, starting from step 4:

4. The pooled representation is flattened to shape  $(n_{\text{envs}}, d \times n_{\text{embedding}})$  and passed into the  $s(\cdot)$  and  $t(\cdot)$  networks, with  $n_{\text{trans}}$  transformations in total. The final output has shape  $(n_{\text{envs}}, n_{\mathbf{z}})$ .

Table 1: Hyperparameter settings for the policy network.

Hyperparameter	Value
Embedding dimension $n_{\text{embedding}}$	32
Number of transformer layers ( $L$ )	4
Key size in self-attention	16
Number of attention heads	8
FFN dimensions	$(n_{\text{embedding}}, 4 \times n_{\text{embedding}}, n_{\text{embedding}})$
Activation	ReLU
Dropout rate	0.05
$\max_{\text{val}}$	10
$\min_{\text{val}}$	-10
$\tau$	$\min(5 \times 0.9995^{\text{step}}, 0.1)$
Initial learning rate	$5 \times 10^{-4}$ (Linear) or $10^{-4}$ (Nonlinear)
Scheduler	ExponentialLR with $\gamma = 0.8$ , step every 1000 training steps
$T$	10 when $d = 10, 20$ 15 when $d = 30$
$n_{\text{step}}$	10000 when $d = 10, 20$ 15000 when $d = 30$
$n_{\text{env}}$ per training step	10

Table 2: Hyperparameter settings for the posterior network in the causal discovery case.

Hyperparameter	Value
Embedding dimension $n_{\text{embedding}}$	128
Number of transformer layers ( $L$ )	8
Key size in self-attention	64
Number of attention heads	8
FFN dimensions	$(n_{\text{embedding}}, 4 \times n_{\text{embedding}}, n_{\text{embedding}})$
Activation	ReLU
Dropout rate	0.05
Bias	-3
Temp	2
Initial learning rate	$10^{-4}$
Scheduler	ExponentialLR with $\gamma = 0.8$ , step every 1000 training steps

The detailed implementation setup is provided in Table 3.

## C.2 Example in Section 5.1

In this example, we consider a fixed causal graph structure with Gaussian priors on parameters:

$$\begin{aligned} \theta_{12} &\sim \mathcal{N}(0.1, 1), & \theta_{23} &\sim \mathcal{N}(1, 0.2^2), & \theta_{35} &\sim \mathcal{N}(0.2, 0.5^2), & \theta_{45} &\sim \mathcal{N}(-0.5, 0.5^2), \\ \theta_{13} &\sim \mathcal{N}(-0.2, 0.5^2), & \theta_{24} &\sim \mathcal{N}(0.3, 0.3^2), & \theta_{36} &\sim \mathcal{N}(0, 0.5^2), & \theta_{56} &\sim \mathcal{N}(0, 0.5^2), \\ \theta_{14} &\sim \mathcal{N}(-0.5, 0.3^2), \end{aligned}$$

with observation model  $X_i = \boldsymbol{\theta}_i^\top \mathbf{X}_{\text{pa}(i)} + \epsilon_i$  where  $\boldsymbol{\theta}_i = [\theta_{ij}]^\top, j \in \text{pa}(i)$ , and additive Gaussian noise  $\epsilon_i \sim \mathcal{N}(0, \sigma_i^2)$  with standard deviations  $\boldsymbol{\sigma} = \{0.2, 0.2, 0.2, 0.2, 0.3, 0.3\}$ . This linear-Gaussian setup enables analytical posterior computations and efficient estimation of the variational lower bound  $\mathcal{R}_{T;L}(\pi; \boldsymbol{\lambda}, \phi)$ .

Figure 8 provides a qualitative assessment of the posterior approximation  $q_\lambda(\mathbf{z}|f_\phi(\mathbf{h}_T))$  achieved by NFs. The NF-based approximations closely align with the true posterior predictive distributions  $p(\mathbf{z}|h_T)$  across these two examples, demonstrating a high-quality posterior approximation.

Table 3: Hyperparameter settings for the posterior network in the causal reasoning case.

Hyperparameter	Value
Embedding dimension $n_{\text{embedding}}$	16
Number of transformer layers ( $L$ )	8
Key size in self-attention	16
Number of attention heads	8
FFN dimensions	$(n_{\text{embedding}}, 4 \times n_{\text{embedding}}, n_{\text{embedding}})$
Activation	ReLU
Dropout rate	0.05
$n_{\text{trans}}$	4
$s(\cdot)$ and $t(\cdot)$ dimensions	(256, 256, 256)
Initial learning rate	$5 \times 10^{-4}$ (Linear) or $10^{-3}$ (Nonlinear)
Scheduler	ExponentialLR with $\gamma = 0.8$ , step every 1000 training steps

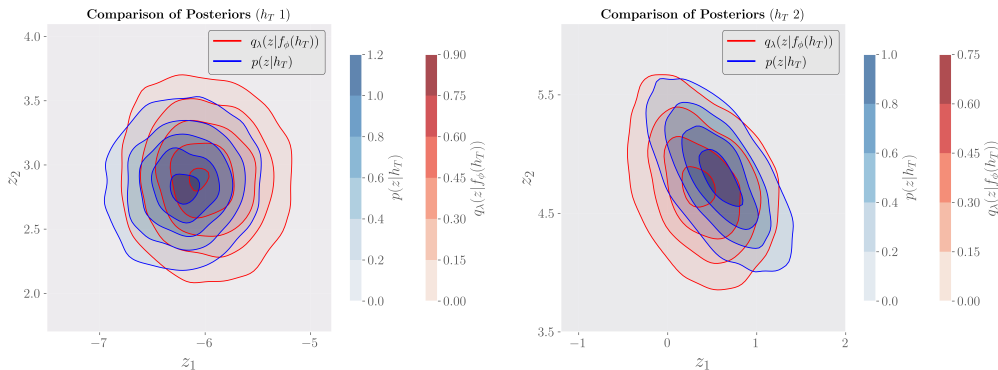


Figure 8: Comparison between the true posterior predictive distribution  $p(\mathbf{z}|\mathbf{h}_T)$  and the variational approximation  $q_\lambda(\mathbf{z}|f_\phi(\mathbf{h}_T))$  for two simulated trajectories. The approximate posterior closely aligns with the true posterior.

### C.3 Examples in Sections 5.2 and 5.3

In the synthetic experiments, we consider Erdős–Rényi (ER) and Scale-Free (SF) random graphs as priors over graph structures. For semi-synthetic experiments, we utilize gene regulatory networks derived from the DREAM benchmarks Greenfield et al. [27], which reflect realistic biological scenarios.

#### C.3.1 Priors over Graph Structures

**Erdős–Rényi** In the ER model, each potential edge between node pairs is included independently with a fixed probability  $p$ . Given  $n$  nodes, the resulting random undirected graph has a number of edges that follows a binomial distribution, with the expected number of edges equal to  $p \times \binom{n}{2}$ . Following Lorch et al. [41], we scale  $p$  such that the expected number of edges is  $\mathcal{O}(d)$ , where  $d$  is the desired average degree. To obtain a DAG, we first retain only the lower triangular portion of the adjacency matrix and then apply a random permutation to the node indices to break symmetry.

**Scale-Free** SF graphs exhibit a power-law degree distribution, where the probability that a node has degree  $k$  is proportional to  $k^{-\gamma}$ , with an exponent  $\gamma > 1$  [6]. Consequently, a small subset of nodes (“hubs”) has a very high number of connections, while most nodes have relatively few. Such structures are commonly observed in biological and social networks. We generate SF graphs using the Barabási–Albert preferential attachment model implemented in NetworkX [28], which iteratively adds nodes by connecting them preferentially to existing high-degree nodes.

**Realistic Gene Regulatory Networks** For semi-synthetic scenarios, we employ networks from the DREAM benchmarks [27], widely used for evaluating computational approaches to reverse-

engineering biological systems. DREAM datasets provide realistic simulations of gene regulatory and protein signaling networks generated by GeneNetWeaver v3.12. Specifically, our experiments focus on two DREAM subnetworks—the *E. coli* and Yeast networks—following the setup described in [60, 41].

### C.3.2 Mechanisms

**Linear Model** In the linear setting, each variable  $X_i$  is modeled as a linear function of its parent variables  $\mathbf{X}_{\text{pa}(i)}$  according to

$$X_i = \boldsymbol{\theta}_i^\top \mathbf{X}_{\text{pa}(i)} + b_i + \epsilon_i, \quad (\text{A12})$$

where  $\epsilon_i \sim \mathcal{N}(0, \sigma^2)$  with fixed variance  $\sigma^2 = 0.1$ . The parameters have priors  $\boldsymbol{\theta}_i \sim \mathcal{N}(0, 2)$  and  $b_i \sim \mathcal{U}(-1, 1)$ .

**Nonlinear Model** For the nonlinear setting, the functional relationship between each child and its parent is modeled using a feedforward neural network with two hidden layers, each containing 8 ReLU-activated neurons. All weights and biases have standard normal priors.

**Queries for Causal Reasoning** For the causal reasoning experiments shown in Figure 3, the query QoIs for the four panels are:  $\mathbf{z} = \{X_6, X_8 \mid \text{do}(X_2 \sim \mathcal{N}(5, 2^2))\}$ ;  $\{X_0, X_5 \mid \text{do}(X_6 \sim \mathcal{N}(3, 1))\}$ ;  $\{X_3, X_5 \mid \text{do}(X_5 \sim \mathcal{N}(6, 0.5^2))\}$ ; and  $\{X_3, X_4 \mid \text{do}(X_9 \sim \mathcal{N}(4, 1))\}$ . For the *E. coli* case in Figure 4, the QoI is  $\mathbf{z} = \{X_6, X_8 \mid \text{do}(X_7 \sim \mathcal{N}(4, 2^2))\}$ .

**Comparison to Discovery-Oriented Policy** To contextualize the performance of GO-CBED- $\mathbf{z}$ , we also include the performance of the structure-learning-oriented policy  $\pi_G^*$ , evaluated on  $\mathcal{R}_{T;L}(\pi_G^*)$ , as shown in in Figures 9 and 10. While GO-CBED- $G$  is effective for causal discovery, it is consistently outperformed by GO-CBED- $\mathbf{z}$  when the objective is to estimate specific causal inquiries, as seen by comparing to Figures 3 and 4.

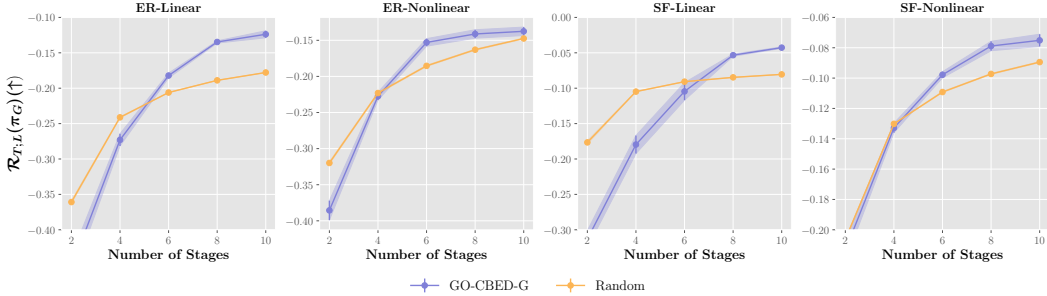


Figure 9: Evaluation of policies on ER and SF graphs with both linear and nonlinear causal mechanisms. The  $\pi_G^*$  demonstrates strong performance in accurately identifying the underlying causal graph across all settings.

## C.4 Incorporating Existing Observational Data into the Prior

In practical settings, it is common to have access to a set of observational data  $\mathcal{D}$  prior to designing interventions. This data can be used to update the prior into a posterior, which then serves as an informative prior for the subsequent experimental design. We infer both the posterior over the graph structure  $p(G|\mathcal{D})$  and the parameters  $p(\boldsymbol{\theta}|\mathcal{D}, G)$  in two stages.

First, since the realized data may not be available during posterior construction, we treat  $\mathcal{D}$  as a random variable. We infer the graph structure using the approach of [41], and train an amortized variational posterior  $q_\lambda(f_\phi(\mathcal{D}))$ , which generalizes across potential realizations of  $\mathcal{D}$ , by minimizing

$$\mathbb{E}_{p(\mathcal{D})} [D_{\text{KL}}(p(G|\mathcal{D}) \parallel q_\lambda(f_\phi(\mathcal{D})))] \quad (\text{A13})$$

with respect to variational parameters  $\lambda$  and  $\phi$ . The approximate posterior  $q_\lambda$  is modeled as a product of independent Bernoulli distributions over potential edges. Once a specific realization  $\mathcal{D}^*$  becomes

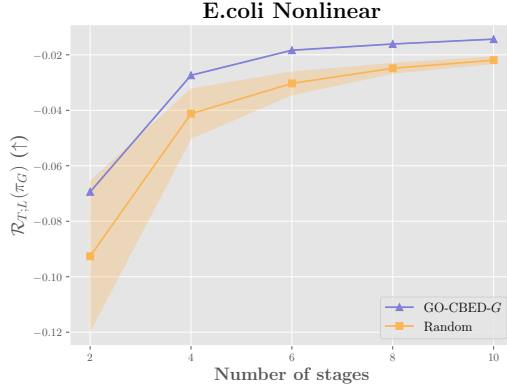


Figure 10: Evaluation of policies on *E. coli* graphs with nonlinear causal mechanisms. The  $\pi_G^*$  demonstrates strong performance in accurately identifying the underlying causal graph.

available, the posterior is instantiated via substitution as  $q_\lambda(f_\phi(\mathcal{D}^*))$ . Samples from this distribution are drawn from the Bernoulli marginals and retaining only acyclic graphs to ensure valid DAGs.

Second, to perform inference over the parameters  $\theta$ , we exploit the conditional independence structure of the posterior:

$$p(\theta|\mathcal{D}, G) = \prod_j p(\theta_j|\mathcal{D}_{\text{pa}(j)}, \mathcal{D}_j, G). \quad (\text{A14})$$

This factorization enables efficient sampling of  $\theta$  by decomposing the joint posterior into node-wise conditionals. For linear models, we sample directly from the posterior  $p(\theta_j|G, \mathcal{D})$  using Markov chain Monte Carlo. For nonlinear models, we apply Pyro’s Stochastic Variational Inference (SVI) [9] to learn a mean-field Gaussian approximation to the posterior.

## D Additional Experiments

### D.1 Higher Bias in the NMC Estimator

We provide a qualitative comparison between the NMC estimator and the GO-CBED approach. The experiment follows the setup in Figure 11, which assumes a fixed graph with  $T = 1$  and additive Gaussian noise  $\epsilon_i \sim \mathcal{N}(0, 0.3^2)$  for all observations. Interventions are uniformly selected in integers from  $-5$  to  $5$ , and the  $\mathcal{R}_T$  or  $\mathcal{R}_{T,L}$  is evaluated using the NMC and GO-CBED estimators and presented in Figure 12. Since there is no policy optimization in this setting, GO-CBED reduces to training a variational posterior network using NFs.

The NMC estimator uses an outer loop size of 5,000 samples, and the inner loop sample size is indicated in the parenthesis in the legend of Figure 12. This sample size is also used as the training sample size for GO-CBED. Despite using significantly fewer samples, GO-CBED consistently identifies the optimal EIG near the boundary of the design space. This finding reinforces our observation from Section 5.1: variational approximations via GO-CBED can offer more efficient and reliable EIG estimation compared to NMC, especially in causal inference tasks involving large graphs or high-dimensional parameter spaces, where traditional sampling becomes computationally and memory intensive.

### D.2 Causal Reasoning on Diverse Realistic Graph Structures

In Section 5.2, we presented causal reasoning results using the *E. coli* gene regulatory network. Here, we extend the analysis to include additional tasks based on both *E. coli* and Yeast gene regulatory networks, each incorporating nonlinear mechanisms. These supplementary experiments further demonstrate the robustness and generality of GO-CBED across a range of causal graph structures and varying complexities of intervention-target relationships (see Figure 13).

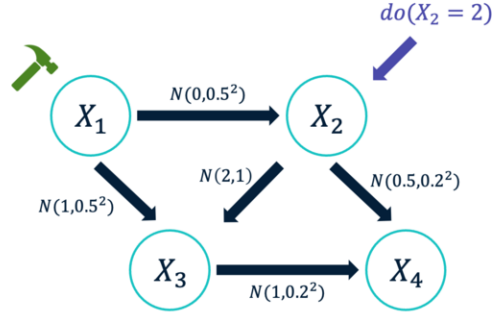


Figure 11: Evaluation of interventions on node 1 using integers from  $-5$  to  $5$ , with the causal query defined as  $z = \{X_3, X_4 \mid \text{do}(X_2 = 2)\}$ .

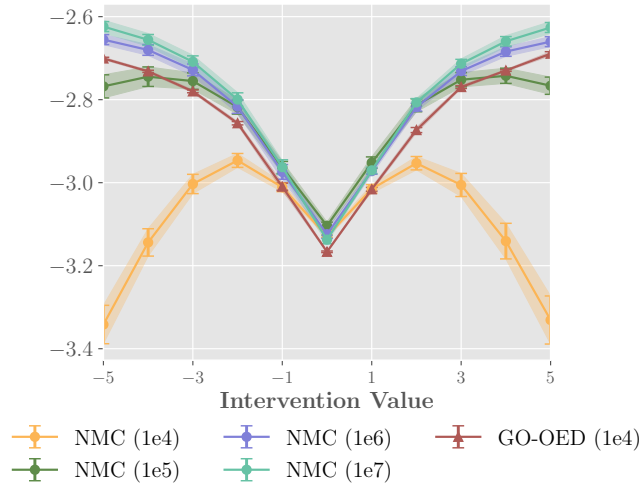


Figure 12: Prior-omitted EIG lower bound estimates, with parenthesis values denoting the inner loop sample size for NMC and training sample size for GO-CBED. Shaded regions represent  $\pm 1$  standard error across 4 random seeds.

Specifically, Figure 13(a) corresponds to the main result in the paper. Figures 13)(b) and (c) illustrate additional scenarios, highlighting GO-CBED’s consistent advantages across diverse topologies. In Figure 13)(b), GO-CBED achieves approximately twice the EIG compared to baselines. This improvement likely stems from the complex paths linking intervention nodes to targets, where goal-oriented strategies more effectively exploit structural dependencies.

In contrast, Figure 13)(c) shows a reduced performance gap. This is likely due to node  $X_5$  being highly informative for both causal discovery and targeted queries, aligning the objective of structure learning and query-specific inference. Notably, the random policy also performs competitively in this setting, likely benefiting from the high-quality variational posterior achievable even under random interventions. We leave a deeper investigation of this phenomenon as an interesting direction for future work.

### D.3 Performance Comparison with Original Posterior Inference Methods

In the main paper, we establish a fair comparison among policies by evaluating them using their respectively pre-trained variational posteriors, thereby isolating the impact of policy optimization. However, a key advantage of GO-CBED is its joint training of both the policy and posterior networks. Specifically, the posterior networks trained in GO-CBED can themselves serve as a highly efficient inference tool, even independent of the policy.

Here, we provide additional results in which each baseline method is evaluated using its original posterior inference procedure, as proposed in their respective papers. Specifically, CAASL [3] uses a

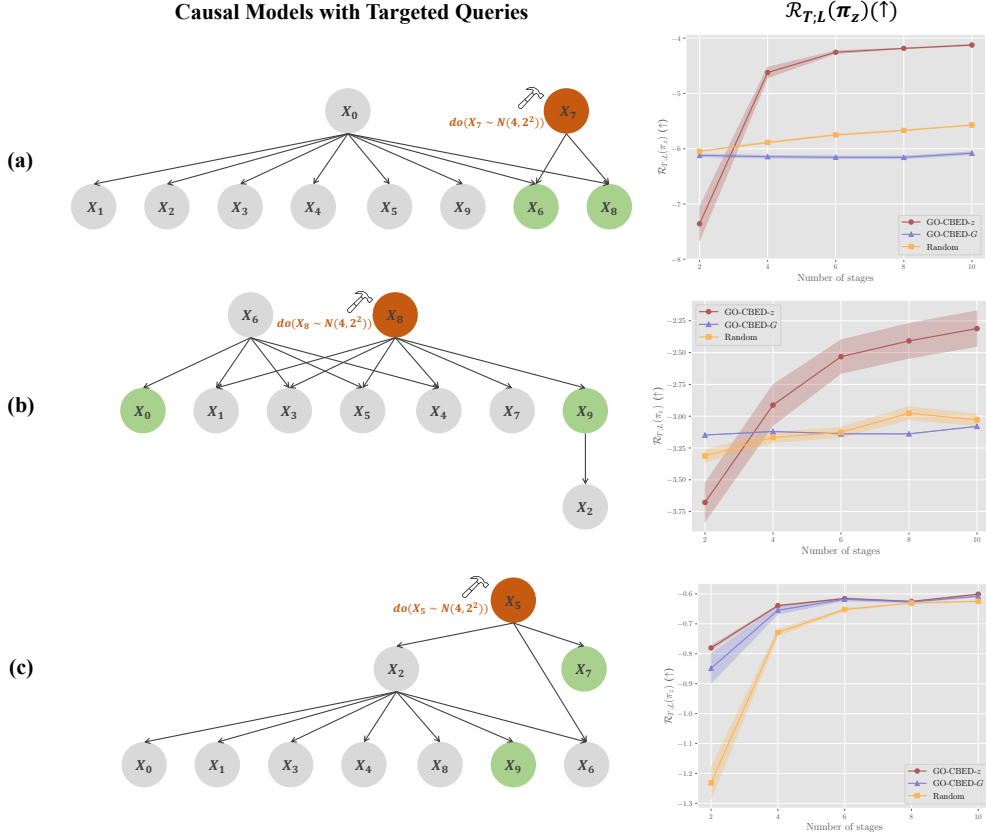


Figure 13: Additional causal reasoning experiments on nonlinear gene regulatory networks. **(a)** *E. coli* network in Section 5.2: intervention on node 7 targeting nodes 6 and 8. **(b)** Yeast network: intervention on node 8 targeting nodes 0 and 9. **(c)** *E. coli* network: intervention on node 5 targeting nodes 7 and 9. GO-CBED consistently outperforms baseline methods, with performance gains varying based on structural complexity of the intervention-target relationships. Shaded regions represent  $\pm 1$  standard error over 4 random seeds.

fixed pre-trained AVICI posterior [40]; DiffCBED [60] and SoftCBED [61] rely on DAG-Bootstrap [21, 29] for linear SCMs and DiBS [40] for nonlinear SCMs.

Figures 14 and 15 present results on synthetic and semi-synthetic SCMs with both linear and nonlinear mechanisms. GO-CBED consistently outperforms baselines across both the  $\mathbb{E}$ -SHD and  $F_1$  score metrics. Interestingly, even the random policy—when paired with pre-trained variational posteriors—achieves competitive performance, highlighting the advantage variational posteriors bring to causal learning.

#### D.4 Extended Evaluation on Causal Discovery Tasks

We extend our analysis with additional causal discovery experiments on more complex settings, with nonlinear mechanisms in *E. coli* networks (Figure 16), and both linear (Figure 17) and nonlinear (Figure 18) mechanisms in Yeast gene regulatory networks. While GO-CBED continues to outperform baseline methods, the performance gap narrows in the nonlinear setting, reflecting the increased difficulty of recovering the full causal structure under complex settings. These results align with our motivation for goal-oriented BOED: when the objective is to answer specific causal queries rather than reconstruct the entire model, targeted policies like GO-CBED-z offer greater efficiency and practical relevance.

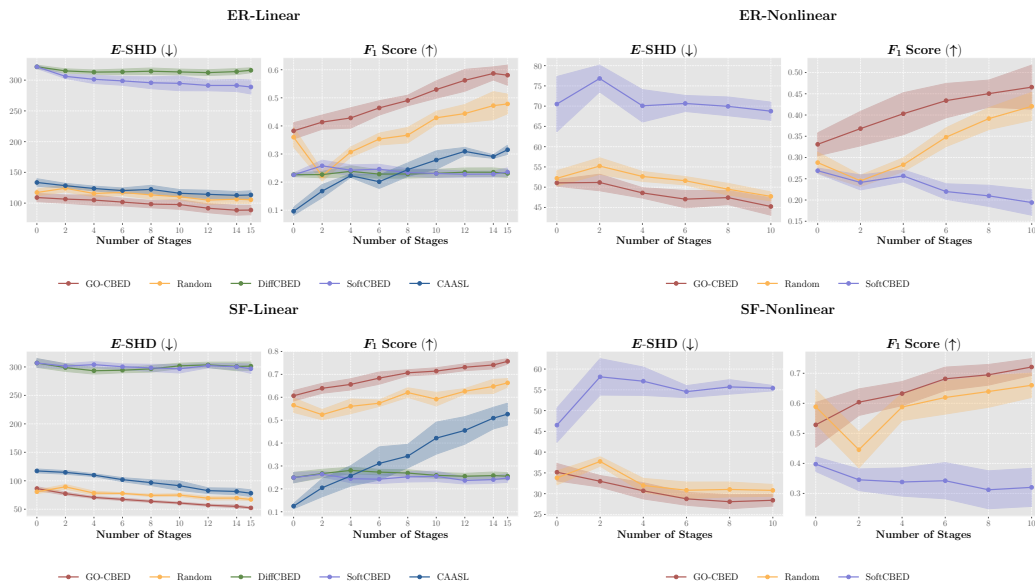


Figure 14: Performance comparison on synthetic SCMs, with each method using its originally proposed posterior inference approach. GO-CBED consistently outperforms all baselines across both linear and nonlinear settings, demonstrating the advantage of jointly optimizing policy and posterior networks. Shaded regions represent  $\pm 1$  standard error across 10 random seeds.

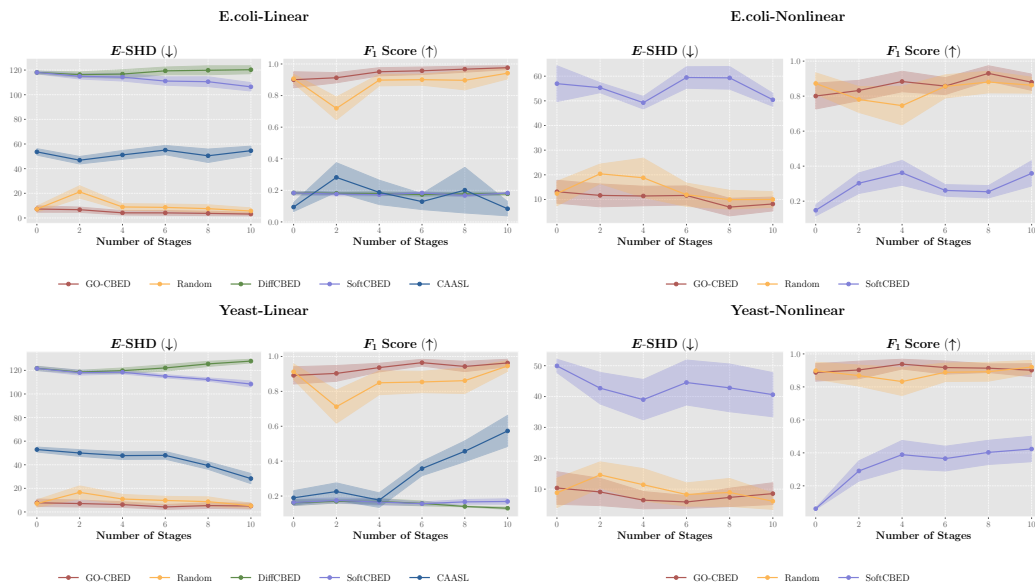


Figure 15: Performance comparison on semi-synthetic gene regulatory (*E. coli* and Yeast) networks, with each method using its originally proposed posterior inference approach. GO-CBED demonstrates strong performance on causal tasks in biologically inspired settings. Shaded regions represent  $\pm 1$  standard error across 10 random seeds.

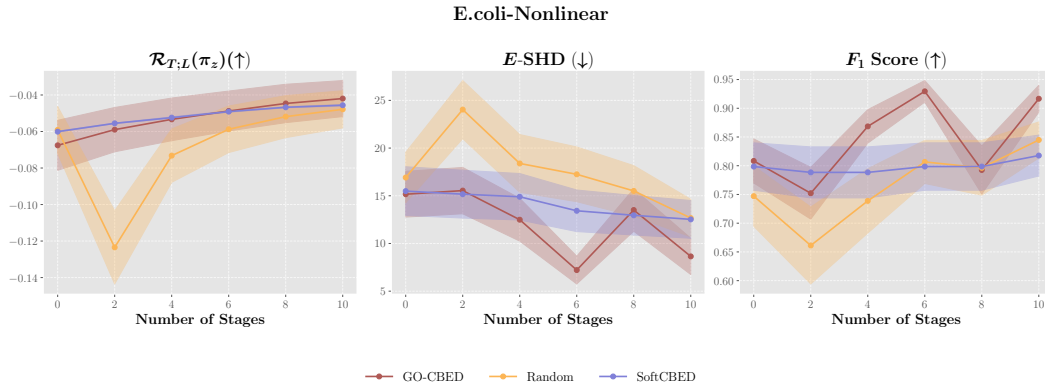


Figure 16: Causal discovery performance on nonlinear *E. coli* gene regulatory networks. GO-CBED performs better or comparatively in terms of uncertainty reduction ( $\mathcal{R}_{T:L}$ ), structural recovery ( $\mathbb{E}$ -SHD), and structural accuracy ( $F_1$ -score) compared to all baselines. Shaded regions indicate  $\pm 1$  standard error across 10 random seeds.

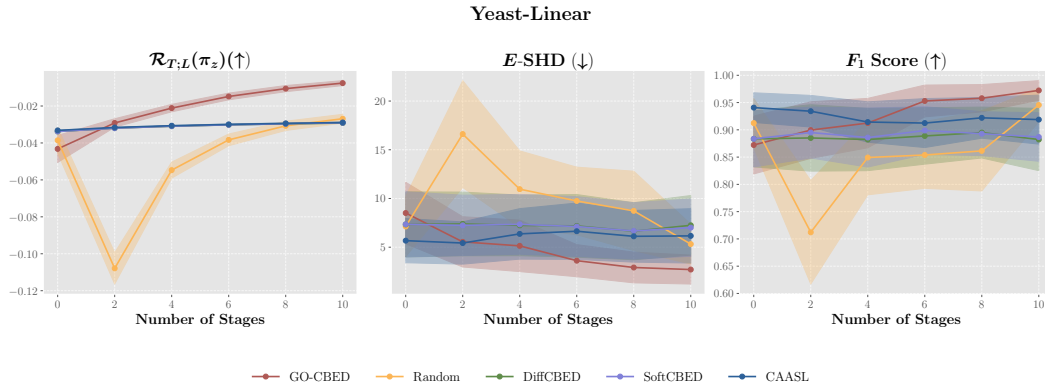


Figure 17: Causal discovery performance on linear Yeast gene regulatory networks. GO-CBED performs better or comparatively in terms of uncertainty reduction ( $\mathcal{R}_{T:L}$ ), structural recovery ( $\mathbb{E}$ -SHD), and structural accuracy ( $F_1$ -score) compared to all baselines. Shaded regions represent  $\pm 1$  standard error across 10 random seeds.

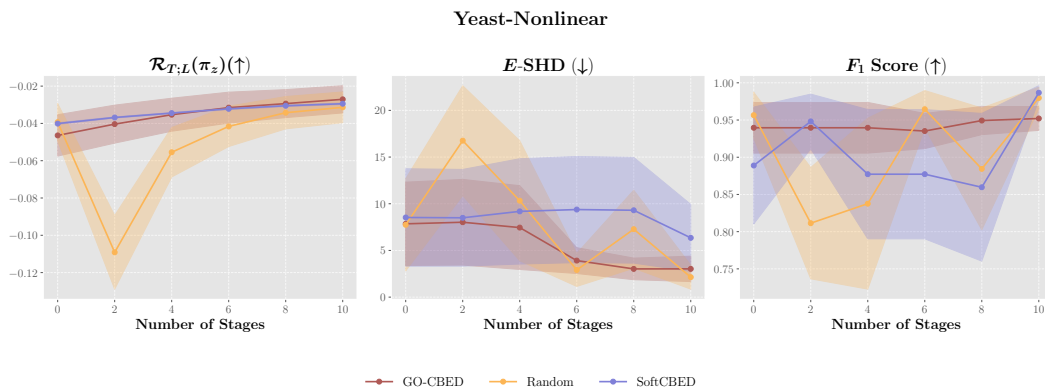


Figure 18: Causal discovery performance on nonlinear Yeast gene regulatory networks. GO-CBED performs better or comparatively in terms of uncertainty reduction ( $\mathcal{R}_{T:L}$ ), structural recovery ( $\mathbb{E}$ -SHD), and structural accuracy ( $F_1$ -score) compared to all baselines. Shaded regions represent  $\pm 1$  standard error across 10 random seeds.

### D.5 Distributional Shift in Observation Noise

We evaluate the robustness of GO-CBED’s policy and posterior networks under distributional shifts in observation noise. At deployment, the noise variance  $\sigma_i^2$  is sampled from an inverse Gamma distribution,  $\sigma_i^2 \sim \text{InverseGamma}(10, 1)$ , in contrast to the fixed variance ( $\sigma_i^2 = 0.1$ ) assumed during training. For comparison, we include a random intervention policy baseline, paired with a posterior network trained specifically on data with the shifted noise distribution.

We first focus on causal reasoning tasks, with ER and SF graph priors over 10-node networks. As shown in Figure 19, GO-CBED consistently outperforms the random baseline, demonstrating the robustness of both its policy and posterior networks in the presence of heteroskedastic noise. In the causal discovery setting (Figure 20), GO-CBED maintains strong performance, demonstrating its reliability across multiple causal tasks and noise conditions.

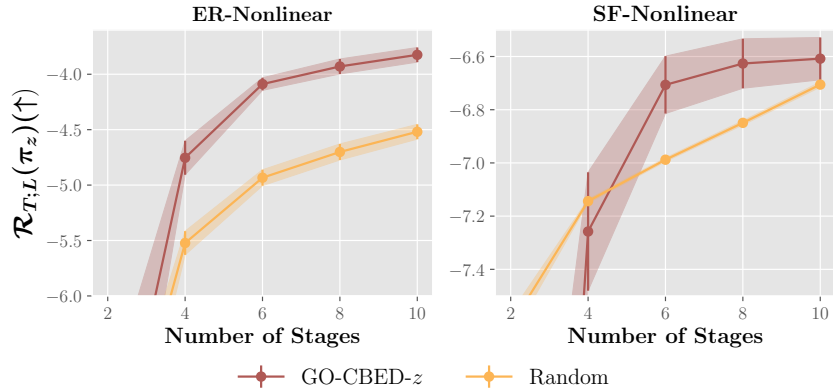


Figure 19: Evaluation of GO-CBED under a distributional shift in observation noise at deployment for causal reasoning tasks. GO-CBED consistently outperforms the random baseline that is using posterior networks pre-trained under the shifted noise, demonstrating the robustness of its jointly optimized policy and posterior networks.

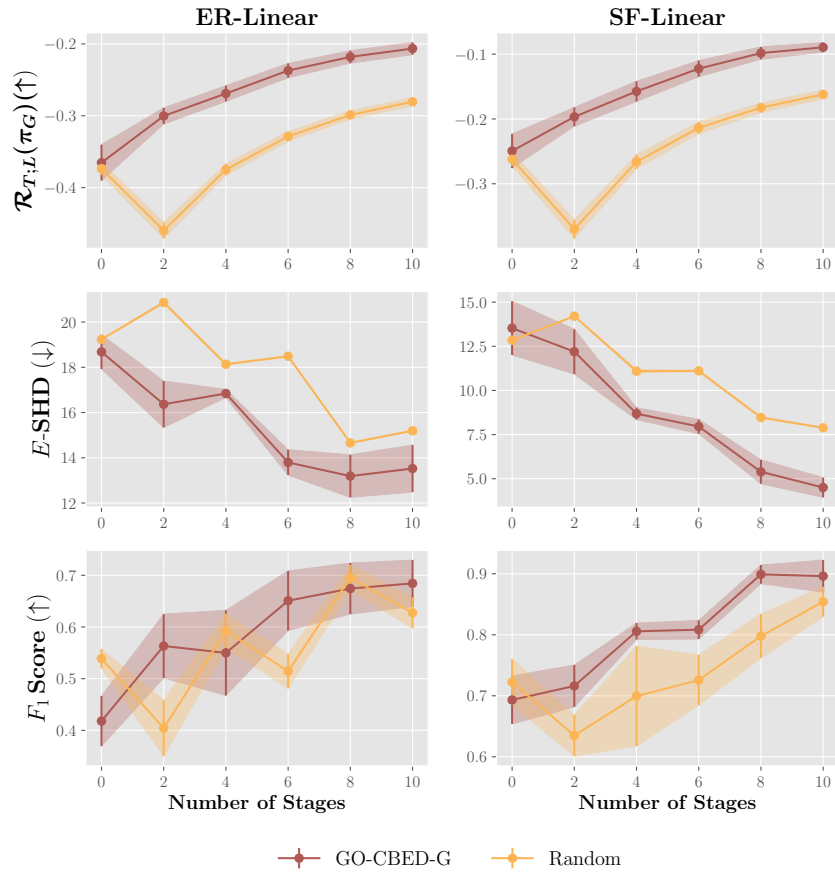


Figure 20: Evaluation of GO-CBED under a distributional shift in observation noise at deployment for causal discovery tasks. GO-CBED consistently outperforms the random baseline that is using posterior networks pre-trained under the shifted noise, demonstrating the robustness of its jointly optimized policy and posterior networks.